

NASA CONTRACTOR REPORT 166567

(NASA-CR-166567) HELISTAT SIMULATION
STUDIES Final Report, Sep. 1979 - Nov. 1982
(Systems Technology, Inc.) 86 p
EC A05/MF A01

N84-20564

CSSL 01C

Unclass
63/08 12045

Helistat Simulation Studies

M. B. Tischler, I. L. Ashkenas



CONTRACT NAS2-10330
November 1982

NASA

NASA CONTRACTOR REPORT 166567

Helistat Simulation Studies

M. B. Tischler
I. L. Ashkenas
Systems Technology, Inc.
Hawthorne, California 90250

Prepared for
Ames Research Center
under Contract NAS2-10330

NASA

National Aeronautics and
Space Administration

Ames Research Center
Moffett Field, California 94035

TABLE OF CONTENTS

	<u>Page</u>
I. INTRODUCTION.....	1
II. SYMMETRIC FLIGHT PERFORMANCE.....	4
III. CROSSWIND PERFORMANCE.....	11
IV. ASYMMETRIC FLIGHT CONDITIONS.....	15
V. LINEARIZED DYNAMICS.....	17
A. Hover Dynamics.....	18
B. Effect of Axial Speed on Dynamics Characteristics.....	30
C. Effect of Sideslip on Dynamics Characteristics.....	35
D. Four-Finned Configuration.....	37
VI. NONLINEAR RESPONSE TO CONTROL.....	42
VII. LANDING CHARACTERISTICS.....	44
VIII. MOORING CHARACTERISTICS.....	46
IX. CONCLUSIONS.....	51
REFERENCES	52
APPENDIX A. HELISTAT SIMULATION INPUT DATA.....	A-1
APPENDIX B. FLIGHT CONTROL CHARACTERISTICS.....	B-1

PRECEDING PAGE BLANK NOT FILMED

LIST OF FIGURES

	<u>Page</u>
1. Nominal Helistat Performance.....	5
2. Helistat Performance with 30,000 lb Slung Payload.....	7
3. Performance Characteristics for Sea Level Based Operations.....	8
4. Performance Versus Payload Weight For Sea Level Based Operations.....	10
5. Crosswind Hover Characteristics.....	12
6. Angular Control Requirements for 15 kt Wind, Varying Sideslip $\psi_w = 0-180$ deg, Nominal Weight Configuration.....	16
7. Pitch Mode, Nominal Configuration; $V_a = 0$	21
8. Pitch Mode, Vehicle/Slung-Load Configuration; $V_a = 0$	25
9. Roll Mode, Vehicle/Slung-Load Configuration; $V_a = 0$	26
10. Pitch Pendulum Mode; $V_a = 0$	28
11. Variation of Surge ($1/T_s$), Heave ($1/T_h$), and Sway ($1/T_{sy2}$) Modes with Axial Speed; Nominal Configuration.....	31
12. Effect of Axial Airspeed on Yaw Instability, $1/T_{sy1}$, for the Nominal and Slung-Load Configurations.....	32
13. Migration of the Pitch Oscillation Mode of the Vehicle (ω_p) and Payload (ω_{1on}) with Axial Airspeed.....	34
14. Migration of Roll Oscillation Mode (ζ_r, ω_r) with Sideslip; Nominal Configuration; $V_w = 15$ kt.....	36
15. Effect of Axial Airspeed on Yaw Instability, $1/T_{sy1}$, <u>4-FINS</u>	38
16. Migration of the Pitch Oscillation Mode (ω_p) with Axial Airspeed, <u>4-FINS</u>	39
17. Response to Lateral Control Input, $\delta_\phi = 0.1$ rad $V_a = 0$, Nominal Configuration.....	43
18. Simulation of Landing Dynamics; 5,000 ft Based Operations.....	45

LIST OF FIGURES (Concluded)

	<u>Page</u>
19. Nonlinear Response of Moored Vehicle to a Discrete Lateral Gust, $V_w = 60$ kts.....	48
a. Helistat Control System--Master Pilot Control Logic.....	B-3
b. Helistat Control System--LPU Control Mixing Logic.....	B-4
c. Helistat Control System--Rotor Longitudinal Cyclic/Propeller Collective Mixing.....	B-5

SECTION I

INTRODUCTION

The Helistat analysis using the heavy-lift airship simulation program package (HYBRDS) covered the following five major areas.

Symmetric Flight Conditions

The basic characteristics of the nominal, maximum and minimum weight configurations without a payload and the nominal weight vehicle with a 30,000 lb payload (Appendix A) were examined in symmetric flight over the speed range of -20 kts to +80 kts. These runs (Run numbers 100 and 200) examined trim control, engine power requirements, and linearized dynamic characteristics. The majority of the study is based on 5000 ft ground level operations. Additional runs were conducted to examine the vehicle characteristics and alternate payload weights for sea level based operations.

Crosswind Hover

The performance of the vehicle in 90 deg crosswind hover conditions was studied (Run numbers 300 and 400) to determine control power requirements and substantial interference effects for the unloaded configuration (nominal, minimum and maximum weight conditions) and the loaded configuration. Special concern was focused on the implications of the roll-to-translate control scheme (Appendix B) on the crosswind hover performance and closed-loop dynamic characteristics of the vehicle.

Asymmetric Flight Conditions

An examination of the sensitivity of the Helistat's dynamic characteristics to changes of sideslip in hover and cruise flight conditions was conducted (Run numbers 500, 600, 700, and 800). In the hover case, the vehicle was trimmed in an inertial wind of 15 kts with varying side-

slip angles from 0 to 180 deg for all unloaded and loaded weight conditions. Additional, sideslip studies were completed for the unloaded and loaded configurations at their respective nominal cruise speeds.

Alternate Configurations

A preliminary study of possible alternate schemes for improving the basic dynamics and performance characteristics of the Helistat was conducted:

- a) Four-finned configurations. The effect of attaching an additional two upper fins (completing the original X-configuration of the envelope) on the basic loaded and unloaded vehicle characteristics (Run numbers 100-4F, 200-4F, and 500-4F, which are the four fin equivalent of basic Run numbers 100, 200, 500). The initial set of runs were conducted assuming no change in the vehicle mass properties. This corresponds to retrimming the ballast and ballonets to hold the vehicle c.g. and weight roughly constant. Additional runs were completed to examine the effect of an aft c.g. shift associated with the addition of two upper fins when the vehicle is not retrimmed.
- b) Roll/Sideforce Mixing. The effect of changing the mixing ratio controlling the relative amount of sideforce and rolling moment generated from pilot lateral stick inputs (Run numbers 200B, 200C, 200D, 300B, 300C, 300D).
- c) Elevator and Rudder Usage. The effect of increasing the relative usage of the tail aerodynamic surfaces for cruise trim control to equalize the rotor thrust levels (Run numbers 100E and 200E).

Time History Analyses

- a) Response to controls. The nonlinear response to lateral stick inputs was calculated to expose dynamic and control characteristics and to assess the validity of linearized models.
- b) One wheel landing. The maximum weight configuration was trimmed in descent to impact the ground with one landing gear. Contractor calculations of landing gear design loads were compared with the simulation results.

- c) Moored vehicle response. The dynamics and loads on the vehicles in the standard mooring (Appendix A) and 4-finned configurations were calculated for ambient wind conditions of 15 and 60 kts (Run numbers THMOR15, THMOR16). Contractor calculations of design mooring loads for extreme atmospheric conditions were compared with the simulation results.

Basic Assumptions

The key assumptions of the Helistat simulation study are:

- 1) The vehicle is assumed to be a rigid body. Deformation of the envelope and interconnecting support structure is ignored. No structural limitations are placed on maximum vehicle attitudes or velocities.
- 2) Control system dynamics are neglected. The control cable and servo dynamics are ignored, so pilot commands are instantaneously translated into surface deflections.
- 3) Engine speed is assumed fixed, thereby maintaining constant rotor and propeller rotational speed (rpm).
- 4) The control system mixing boxes are assumed to allow limiting of 1 or more surfaces (e.g., rotor cyclic propeller collective, etc.) without restricting control over the remaining (non-limited) surfaces. For example, forward propulsion commands (BISC, Appendix B) produce mixed deflections of propeller collective and rotor longitudinal cyclic. After the rotor cyclic reaches its limit (12.5 deg), additional propulsion commands generate increased propeller collective deflection until the propeller deflection limit is reached.
- 5) All hover and cruise performance studies assume a zero pitch attitude (level flight) orientation. The free stream angle-of-attack is also zero, although induced flow angles are generated by the various interference effects (Ref. 1).
- 6) The ballonets are not used to trim the pitch attitude of the vehicle (except for the 4-Finned, nominal c.g. case, Section V, Subsection D). Note that the mass characteristics of the nominal and slung-load configurations are based on flight at the pressure ceiling (ballonets fully deflated, Appendix A).

SECTION II

SYMMETRIC FLIGHT PERFORMANCE

The performance of the Helistat without control limiting effects is shown in the solid lines of Fig. 1. This analysis is based on the nominal weight condition at a 6000 ft pressure height.

With the average rotor collective setting nearly constant at 40 percent of the maximum deflection, the control mixing laws (Appendix B) allocate roughly constant lift power to the rotors, reserving axial propulsion power for the propellers. The total required shaft horsepower (rotor and propeller) is seen to be fairly constant in the speed range of -20 to +20 kts, with sharp increases for flight speeds exceeding 40 kts. Assuming a flat rated normal operating power of 1275 hp per engine, (Ref. 2) the cruise speed of the Helistat at 6000 ft is about 50 kts. This leaves the remaining 1000 horsepower (250/engine) for maneuvering flight. Also shown in this figure are the speeds for maximum endurance, (17 kts) and maximum range (32 kts). The somewhat unusual "kink" in the propeller and total power curves around 50 kts results from the increased trim pitching moment of the interconnecting structure at the high forward speeds, giving rise to asymmetric (inefficient) rotor/propeller mixing (Appendix B).

The effect of rotor longitudinal cyclic limiting at a swash plate angle of 12.5 deg is shown in the dotted lines of Fig. 1. When the rotor longitudinal cyclic limits are encountered, rotor shaft horsepower requirements remain roughly constant and the excess horsepower capability is absorbed by the propellers. The total power curve has a steeper slope than before near the maximum takeoff power level, suggesting a decrease in the available control margin at the 50 kt cruise condition.

The nose-up pitch trim ($\delta\theta$) is reduced when power is diverted to the propellers, because of the low propeller thrust line relative to the vehicle center-of-gravity. This results in more equalized rotor thrust levels with associated symmetrical rotor/propeller mixing and the elimination of the undesirable "kink" in the total power curve at 40 kts.

ORIGINAL PAGE 19
OF POOR QUALITY

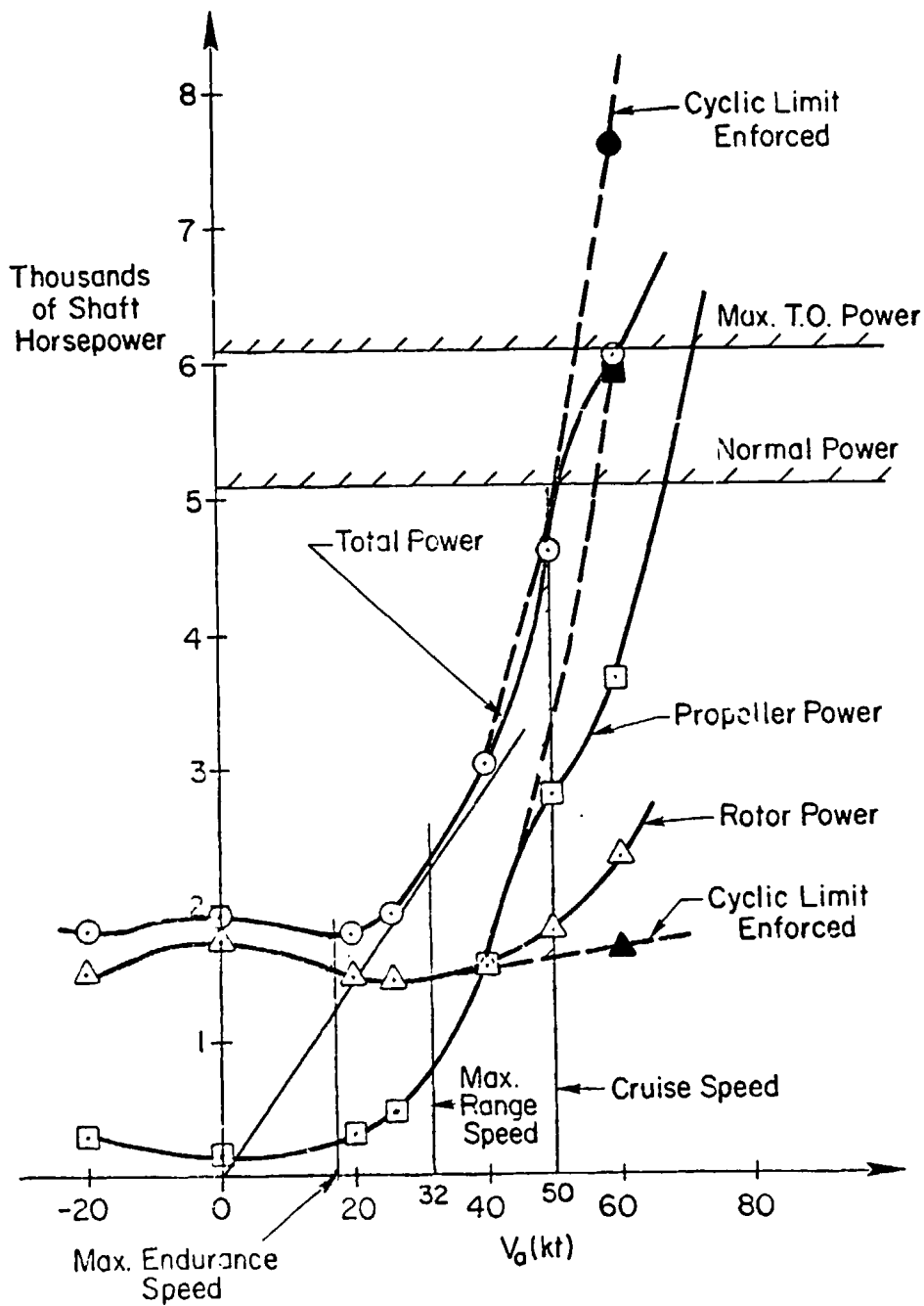


Figure 1. Nominal Helistat Performance

This equalization in rotor thrust levels is also achieved by increasing the relative usage of the tail aerodynamic surfaces for cruise trim control.

The performance of the Helistat with a 30,000 lb slung payload (including payload drag and cable deflection, Appendix A) is shown in Fig. 2 for the 6000 ft pressure ceiling condition. The engine power is diverted almost entirely to the rotors, since the rotors are operating at 80 percent of their maximum collective setting (Appendix B). Only a minimal power is reserved for overcoming the profile drag associated with the free spinning propellers. The normal rated power level gives a maximum cruise speed of about 46 kts; however the steepness of the power curve in this speed regime suggests a reduced operational cruise speed of about 40 kts, to allow a somewhat larger control margin capability. The 40 kt speed roughly corresponds to the speed for maximum range which may be a desirable cruising condition for typical operations.

When the swash plate deflection limits are considered, rotor longitudinal cyclic limiting occurs at a speed of 35 kts. As shown in the dashed lines of Fig. 2, the remaining engine power can be absorbed in the propellers, resulting in almost identical power performance of the loaded vehicle up to 60 kts. As before, the slightly improved power characteristics of the vehicle in the 50 kt region are due to the equalization of the rotor thrust levels.

Although not specifically shown in Fig. 1, performance calculations for the minimum and maximum weight configurations indicate that the cruise speeds remain roughly at 50 kts, indicating only small changes in the (cruise) performance of the vehicle with loading condition. As later shown, however, the hover power requirements are much different, as expected.

The performance curves for sea level based operations (cruise at ballonet ceiling of 1,000 ft above sea level) are shown in Fig. 3 for the nominal and sling-load configurations. The lower cruise altitude yields an increase in buoyancy ratio ($\beta = 0.89$) compared to the 6,000 ft level ($\beta = 0.78$). This results in lower trim rotor thrust requirements,

ORIGINAL PAGE 17
OF POOR QUALITY

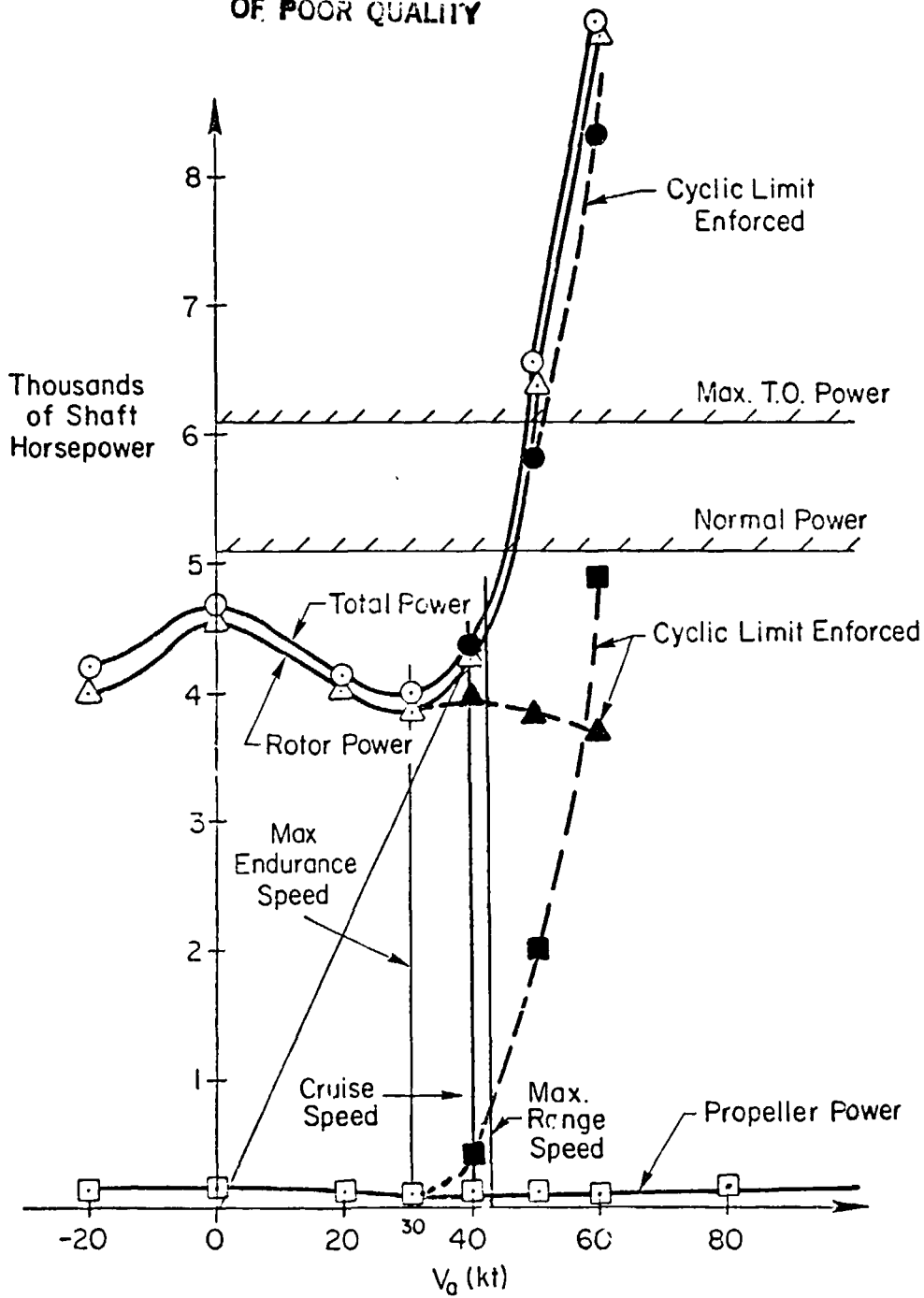


Figure 2. Helistat Performance with 30,000 lb Slung Payload

ORIGINAL FACTOR
OF POOR QUALITY

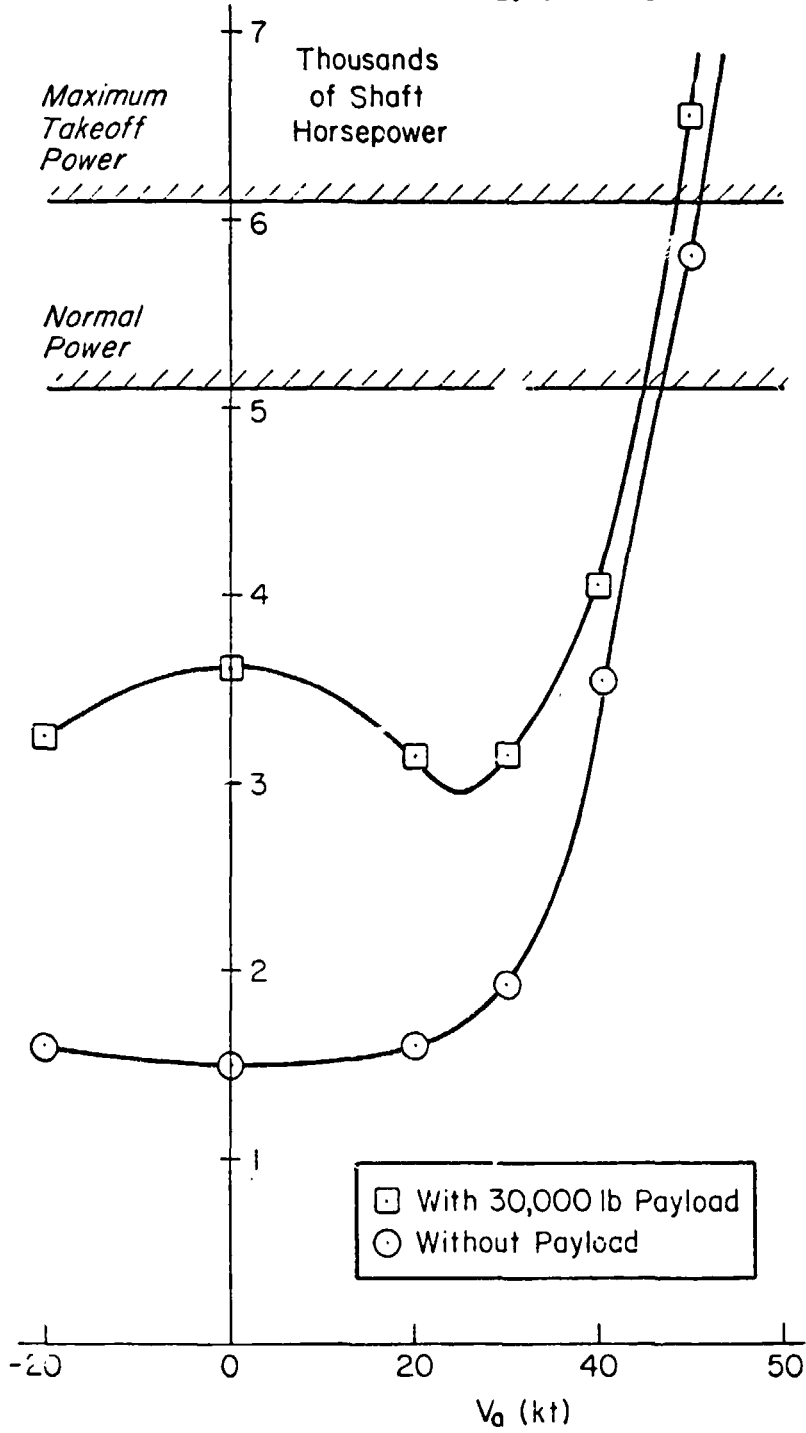


Figure 3. Performance Characteristics for Sea Level Based Operations

which combined with the improved low altitude rotor efficiency, yields a 25 percent reduction in hovering power for the unloaded and loaded configurations (compare Figs. 1 and 2 vs. Fig. 3). The increased parasite drag resulting from the higher air density causes the power curves at the higher airspeeds to be steeper than before. In order to allow for some maneuvering margin, the cruise speed for the unloaded configuration is reduced by about 10 kts to 40 kts, roughly the same as the cruise speed for the sea level-based slung-load configuration.

The effect of varying payload weight on hover and (40 kt) cruise performance is shown in Fig. 4. These results are for sea level based (1000 ft) operations. Since the power required for hover is composed almost entirely of the induced power due to rotor lift, the (hover) curve follows a 3/2 exponent law:

$$h_{\text{Phover}} \doteq h_{\text{pinduced}} = \frac{T v_i}{550} \quad (1)$$

$$v_i \doteq \sqrt{\frac{T}{2\rho A}} \quad (2)$$

$$h_{\text{Phover}} \propto T^{3/2} \propto W_{\text{pay}}^{3/2} \quad (3)$$

This result is confirmed in Fig. 4. The operational payload limit in hover is 46,500 lb. As previously noted, the cruise power is dominated by parasite drag, so the effects of varying payload weight at the cruise speed (40 kts) is small (Fig. 4). The maximum payload capability in cruise is 45,000 lb, representing the limit for sea-level based operations.

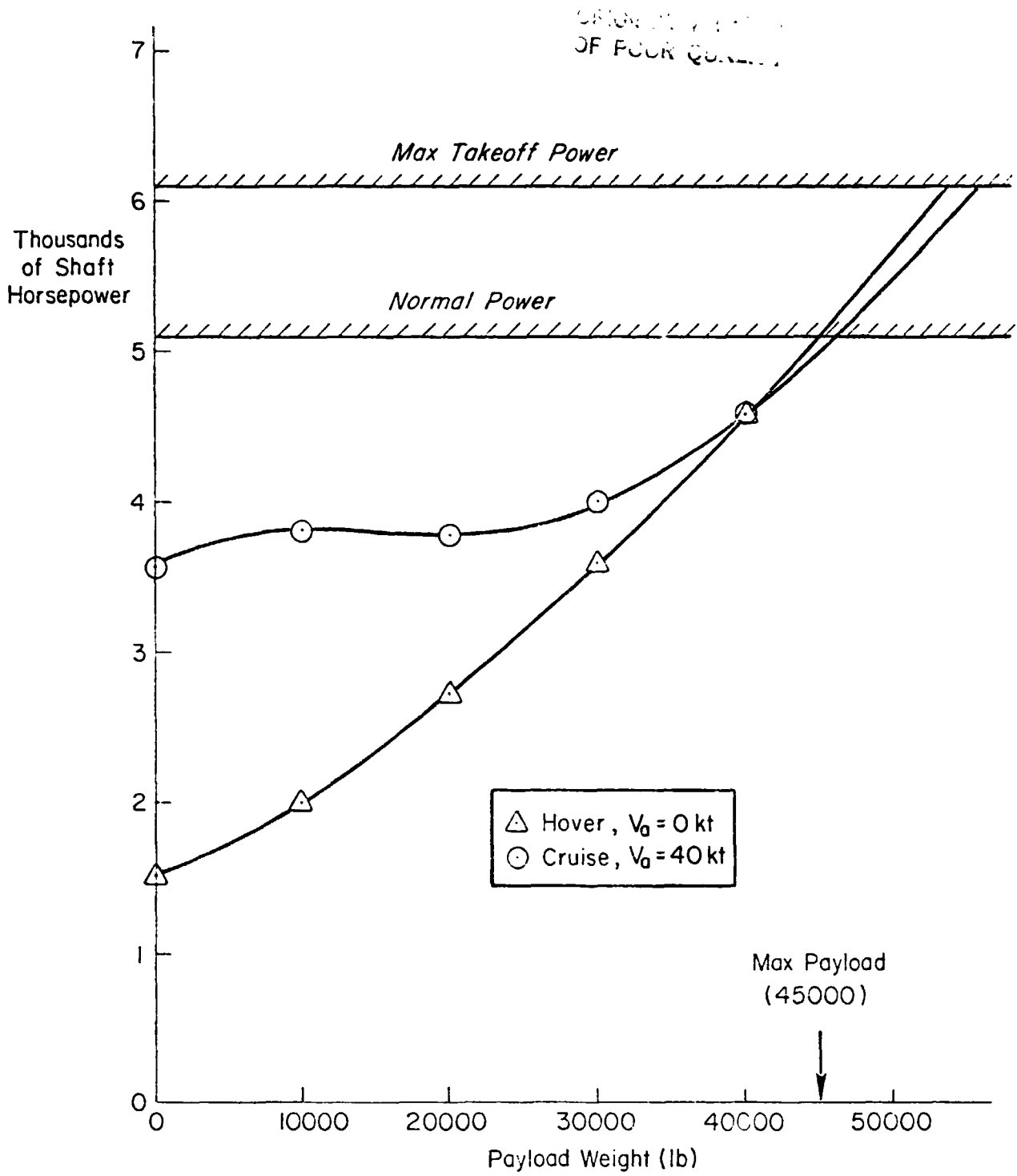


Figure 4. Performance Versus Payload Weight For Sea Level Based Operations

SECTION III

CROSSWIND PERFORMANCE

The crosswind hover performance of the unloaded and loaded vehicle for standard (5,000 ft based) operations is shown in Fig. 5. This figure presents the trim roll angle (degrees) as a function of crosswind velocity (knots). For the unloaded configuration, the maximum crosswind capability is restricted to 15 kts by the minimum collective settings on the upwind rotors (0.5 deg), and maximum collective (12.5 deg) and lateral cyclic (12 deg) settings on the downwind rotors. This results in a trim roll angle of 40 deg. For the loaded configuration, the maximum obtainable crosswind capability is 10 kts due to maximum collective and power limiting on the downwind rotors (1 and 3). The corresponding trim roll angle is 9 deg.

The maximum crosswind trim conditions of 10 and 15 kts for the loaded and unloaded flight configurations respectively, do not allow any additional maneuvering control margin. A design guideline for quadrotor HLA's to maintain hover in an ambient wind of 20 kts at 30 deg sideslip angle has been proposed by NASA (Ref. 3). This yields a crosswind requirement of 10 kts. The unloaded Helistat can achieve this requirement with some additional control margin for gust suppression and maneuvering. For similar control margins, the loaded configuration will be limited to 5-8 kts crosswind, or about a 20 deg sideslip angle for a 20 kt wind condition.

It is unlikely that the ZPG-2 envelope will maintain the large roll angles implied by this (rigid-body) analysis without deforming. Gross distortions of the hull and catenary curtain system may significantly degrade the 40 deg/15 kt upper limit shown in Fig. 5. Additional constraints will likely result from the allowable minimum clearance between the deformed envelope and the downwind rotors. Significant increases in the hull on rotor interference effects on the downwind rotors may further erode the crosswind capability of the unloaded configuration.

OF FLOOR CONTROL

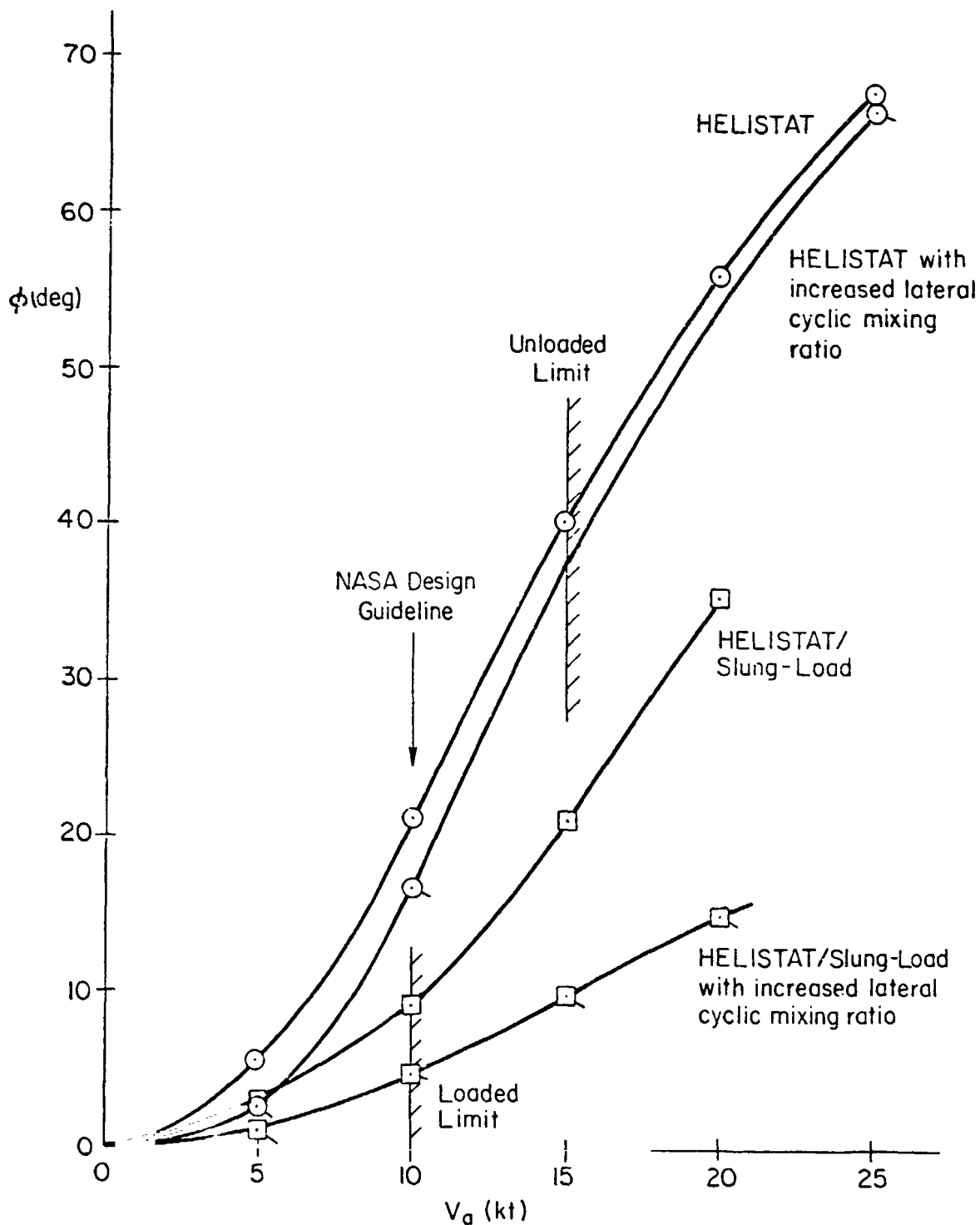


Figure 5. Crosswind Hover Characteristics

The large roll angles which result from the roll to translate logic also suggest a number of possible handling quality related problems. Since the vehicle is not in a coordinated turn, these angles will result in a very uncomfortable pilot environment in which steady lateral g's may degrade precision hand and foot coordination and control. In addition, such roll attitudes may preclude the pilot from seeing the payload hook during pickup operations. In manual control terms, the roll-to-translate logic may make simultaneous pilot closure of attitude and position loops very difficult since the pilot's lateral location 65 ft from the hull c.g. will couple roll attitude and vertical position cues. The pilot will undoubtedly be closing manual control loops around feedback cues at his own position, and may not be able to distinguish between roll (and pitch) attitude disturbances and vertical position disturbances. In fact, since attitude changes cause rigid body vertical translations of the pilot position, the pilot may (if untrained) initially attempt to use the heave controller to regulate against attitude (and heave) disturbances. Such coupled cues and responses could significantly degrade the closed-loop bandwidth of the system and threaten operational safety. Another problem with the roll-to-translate logic, which has been reported in Heavy-Lift Helicopter (HLH) studies (Ref. 4), is the undesirable excitation of the payload pendulum mode. Large induced motions of the unloaded cable hook caused by lateral inputs would also be especially troublesome during load pickup operations.

A desirable solution would be a control law which yields small roll angles for precision lateral input (± 5 kt) in zero sideslip conditions and large rolls angles for maximum crosswind capability in critical situations. This could be accomplished by increasing the ratio of lateral cyclic to roll control usage for lateral stick inputs. Figure 5 (flagged symbols) shows the crosswind results when the lateral cyclic gain is increased by a factor of 5. The loaded and unloaded configurations exhibit 50 percent reductions in the trim roll angle for a 5 kt crosswind condition. In the unloaded case, the lateral cyclics limit at about 8 kts, with further lateral stick inputs resulting in quickly increasing roll angles. The maximum trimmable crosswind remains at



15 kt ($\phi = 37.5$ deg) due to both collective and cyclic limiting, as before. For the loaded vehicle, the maximum trimmable crosswind remains at 10 kts because of simultaneous lateral cyclic (sideforce) and downwind rotor power (roll control) limiting.

Some additional improvement in the crosswind characteristics of both loading conditions could be achieved by eliminating the use of differential lateral cyclic for yaw control. Since both longitudinal cyclic and propeller collective are available for the purpose, and the close fore-aft rotor spacing makes lateral cyclic fairly ineffectual for yawing moment generation, this change would not significantly reduce maximum yaw control capability.

SECTION IV

ASYMMETRIC FLIGHT CONDITIONS

When the vehicle is oriented with angles-of-attack or incidence relative to the local wind, large (unstable) hull aerodynamic moments result. In these flight conditions, trim and maneuver control margins become severely limited. The pilot controls (δ_ϕ , δ_θ , δ_ψ) required to trim the nominal (unloaded) configuration in a 15 kt ambient wind are shown as a function of wind sideslip angle (ψ_w) in Fig. 6 (these results are for the vehicle fully trimmed in all degrees-of-freedom). The roll control (δ_ϕ) reaches a maximum in the crosswind condition ($\psi_w = 90$ deg), as expected. The yaw control is zero and has a stable slope when $\psi_w = 76$ deg, the angle of sideslip where the hull and tail yawing moments are balanced. The yaw control (δ_ψ) reaches a maximum at $\psi_w = 135$ deg, corresponding to the wind angle for maximum (unstable) static yawing moment. The effect of the large combined roll and yaw control requirements results in asymmetries in the rotor/propeller mixing functions, which in turn cause large pitch control requirements (δ_θ) around $\psi_w = 120$ deg (Fig. 6).

Thus, the wind angle range of $\psi_w = 105$ - 135 deg is critical for angular trim control of the Helistat. Changes in vehicle operating weight and payload have only a secondary effect on these results. Moreover, the results to be presented in the next section suggest associated problems in dynamic roll response for flight in this region. Therefore, sustained flight in the 105-135 sideslip condition should be avoided.

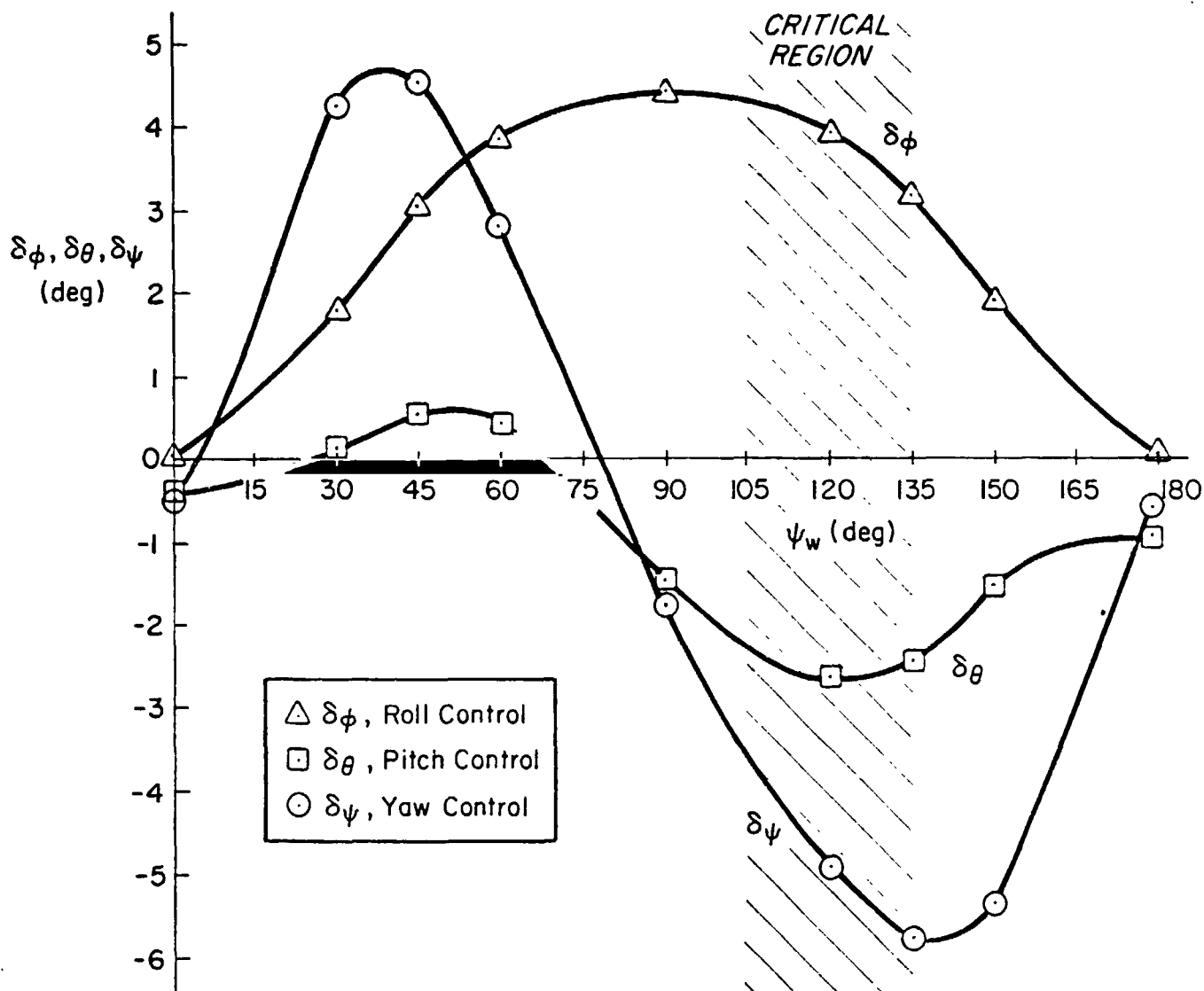


Figure 6. Angular Control Requirements for 15 kt Wind, Varying Sideslip $\psi_w = 0-180$ deg, Nominal Weight Configuration

SECTION V

LINEARIZED DYNAMICS

The dynamic equations of motion are numerically linearized to obtain the following first order linear differential equation,

$$\dot{\underline{X}} = \underline{A}\underline{X} + \underline{B}'\underline{U} + \underline{C}\underline{G} \quad (4)$$

where \underline{X} is the state vector of vehicle and payload linear and angular positions and rates. Vehicle motions are referenced to the hull c.g., nominally located 14.4 ft below the hull center of volume (Appendix A). Linear and angular velocities (u, v, w, p, q, r) are relative to rotating body-fixed (hull) axes. Linear positions (x, y, z) are given in inertial frame Cartesian coordinates, and angular orientation is given in inertially based Euler coordinates (ϕ, θ, ψ). Payload motions are referenced to the payload c.g., nominally located 12.6 below the cable hook attachment point. Linear payload velocities and positions ($u_p, v_p, w_p, x_p, y_p, z_p$) are relative to the hull, while the angular velocities and orientations ($p_p, q_p, r_p, \phi_p, \theta_p, \psi_p$) are relative to inertial space. These various axis systems are fully described in Ref. 1.

The superscript "o" in Eq. 4 denotes the first derivative of the state vector with respect to the rotating axes. \underline{U} is the five element vector of pilot cockpit controls. \underline{G} is the gust state vector of air mass linear and angular velocities. \underline{A} , \underline{B}' and \underline{C} are the stability derivative matrices. Taking the Laplace transform of Eq. 4,

$$[sI - \underline{A}]\underline{X}(s) = \underline{B}'\underline{U}(s) + \underline{C}\underline{G}(s) \quad (5)$$

where s is the Laplace Operator and I is the identity matrix. The natural (unforced) motion of the vehicle is obtained by setting the control and input vector to zero,

$$[sI - A]\underline{X}(s) = \underline{0} \quad (6)$$

The solution of the unforced motion has the form

$$\underline{X}(t) = \underline{X}_1 e^{\lambda_1 t} + \underline{X}_2 e^{\lambda_2 t} + \underline{X}_3 e^{\lambda_3 t} + \dots + \underline{X}_n e^{\lambda_n t} \quad (7)$$

where $\underline{X}_1, \underline{X}_2, \underline{X}_3, \dots, \underline{X}_n$ are the eigenvectors associated with each eigenvalue ($\lambda_1, \lambda_2, \lambda_3 \dots \lambda_n$). In the case of the unloaded vehicle, there are twelve characteristic eigenvalues and twelve associated eigenvectors. For the loaded vehicle, there are an additional twelve eigenvalues associated with the dynamics of the slung payload.

The eigenvalues of the system provide information on the time constants and relative stability, while eigenvectors illustrate the relative magnitudes and phasing of the elements of the state vector, \underline{X} , in each of the various modes of motion. From Eq. 7 it is apparent that if a characteristic root has a positive sign (e.g. $\lambda_1 > 0$), then the mode associated with its response ($\underline{X}_1 e^{\lambda_1 t}$) is unstable and the corresponding motion will grow with time. When the root is negative (e.g., $\lambda_1 < 0$), the associated mode is stable and the corresponding motion will die out with time. The following sections discuss the characteristic modes of motion of the vehicle and payload and consider their sensitivity to axial and asymmetric flight conditions.

A. HOVER DYNAMICS

The unloaded vehicle exhibits five characteristic modes of motion:

- 1) Surge Subsidence ($1/T_s$)
- 2) Heave Subsidence ($1/T_h$)
- 3) Pitch Oscillation (ζ_p, ω_p)
- 4) Coupled Sway-Yaw ($1/T_{sy1}, 1/T_{sy2}$)
- 5) Roll Oscillation (ζ_r, ω_r)

Surge Subsidence ($1/T_s$). This stable mode is a 1 degree-of-freedom motion comprised of axial speed perturbations. The long surge-mode time

constant ($T_g = 151.5$ sec) is due to the small level of hull drag and rotor damping relative to the large effective axial mass. This very low frequency mode suggests potential problems in maintaining position in the presence of axial disturbances. Surge motions are largely decoupled from the pitch motions because the speed derivatives, M_u and Z_u are small in the hover flight condition. This is unlike the conventional hovering dynamics for helicopters which involves coupled variations of speed and attitude. The eigenvectors associated with the surge mode indicate coupling between the longitudinal and lateral degrees of freedom due to rotor lateral flapping in response to longitudinal speed perturbations (Y_u). The modal response ratio for the unloaded hovering flight condition is

$$|v_{hcg} : u_{hcg}|_{1/T_g} = |0.26:1|$$

This interaxis coupling suggests possible difficulties in the manual stationkeeping task because of the need for pilot crossfeeds.

Heave Subsidence Mode ($1/T_h$). This stable mode is predominantly composed of vertical motion and derives its damping from the rotors. The rotor flapping dynamics induce some coupling between heave and surge motions, the modal response ratio being,

$$|u_{hcg} : w_{hcg}|_{1/T_h} = |0.13:1|$$

For the nominal unloaded flight condition, the heave mode frequency ($1/T_h = 0.0866$ rad/sec) is significantly lower than typical values for single rotor helicopters in hover ($1/T_{h\text{typical}} \doteq 0.25 - 0.5$ rad/sec). This is due to the large effective vertical mass (inertial + vertical apparent mass) relative to the trim rotor thrust levels. Recent VSTOL studies on flight path handling qualities (Ref. 5) indicate minimum acceptable heave mode frequencies of about 0.3 rad/sec for precision path control, suggesting possible vertical stationkeeping problems for the Helistat.

Pitch Oscillation (ζ_p, ω_p). The pitch oscillation mode is comprised of variations in axial speed and pitch rate. The eigenvector diagram of

Fig. 7 shows the relative magnitude and phasing of the major components of this mode. A time history of the vehicle motion within this mode is obtained by rotating the vectors counter-clockwise about the origin with a frequency of $\omega_p = 0.29$ rad/sec (indicated by the arc in Fig. 7), and plotting the magnitude of the vector projection on the real (σ) axis multiplied by the exponential ($e^{-\zeta_p \omega_p t}$). The reader is referred to Ref. 7 for a more detailed discussion of eigenvalue-eigenvector techniques. Axial translation and pitching motions are roughly in phase, the modal response ratio being,

$$|\theta_h : x_{h_{cg}}|_{\omega_p} = 10.83^{\circ} : 1 \text{ft}$$

The frequency of oscillation ($\omega_p = 0.29$ rad/sec) is determined by the metacentric height (the height of the hull center of volume above the vehicle center of gravity) and the effective pitch inertia. The damping ratio for the hover flight condition ($\zeta_p = 0.069$) results from roughly equal contributions of the hull and rotors. The dynamics of the Helistat pitch oscillation mode is similar to a 1 deg-of-freedom pendulum motion and is not related to the pitch/speed oscillation exhibited by most VSTOL aircr. ft.

The eigenvector results of Fig. 7 yield an instantaneous center of rotation for unforced pitch motion located approximately 18 ft above the top of the hull envelope (55 ft above the hull center of volume). Tight piloted stabilization of the pitch oscillation mode will be essential to maintaining accurate hook position since the vertical separation between the unforced pitch center-of-rotation and the cable attach point is considerable (107 ft).

Coupled Sway-Yaw ($1/T_{sy_1}$, $1/T_{sy_2}$). This mode is comprised of coupled variations in side velocity and yaw angle. The dynamics of the coupled sway-yaw mode for the unloaded case are stable and occur at very low frequencies ($1/T_{sy_1} = 0.0103$ rad/sec, $1/T_{sy_2} = 0.0108$ rad/sec). These modes depend on the yawing moment characteristics, lateral hull drag and rotor damping. As the axial velocity increases, the unstable static yawing moment characteristics cause a wide separation of these

ORIGINAL PAGE IS
OF POOR QUALITY

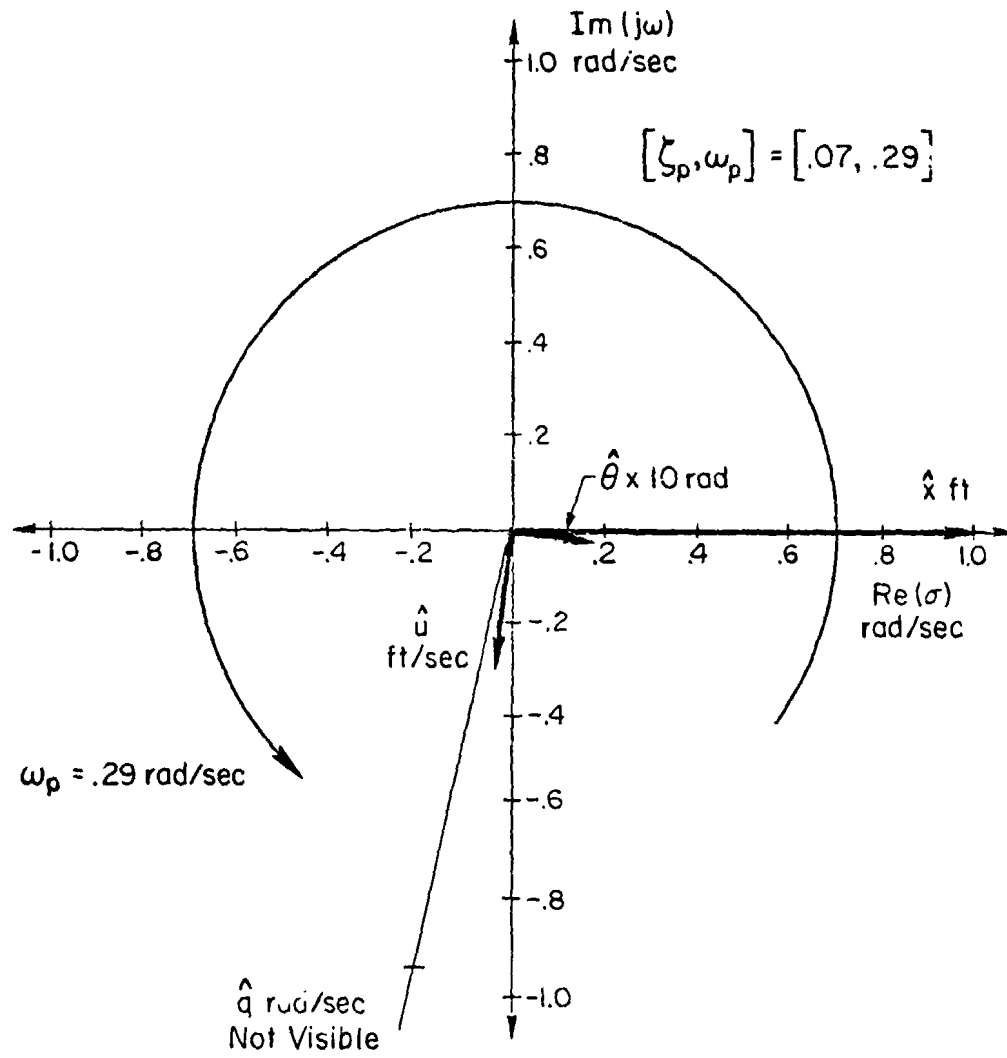


Figure 7. Pitch Mode, Nominal Configuration; $V_a = 0$

roots with a resulting unstable root ($1/T_{sy1}$) associated with yawing motions and the stable root ($1/T_{sy2}$) associated with lateral sway motions. As noted in the discussion of the surge mode, the rotor flapping dynamics induce some coupling between lateral and longitudinal degrees of freedom. For the hover case, sway-yaw oscillations induce axial motions of approximately 23 percent, a result which is directly analogous to the surge results.

Roll Oscillations (ζ_r, ω_r). The stable oscillatory roll mode is a well damped 1 DOF pendulum motion comprised of perturbations in side velocity and roll angle. In hover, the roll mode is the lateral equivalent of the pitch oscillation mode discussed earlier. The natural frequency ($\omega_r = 0.51$ rad/sec) is controlled by the metacentric height and effective roll inertia. The damping ratio ($\zeta_r = 0.164$) is greater than in the pitch mode due to the increased ratio of damping moment to moment of inertia (L_p). The roll center of rotation obtained from the modal response characteristics, is approximately coincident with the hull center of volume. This mode may be well represented by 1 DOF rolling motions about the hull center of volume axis.

The frequency and damping characteristics of the roll mode suggest that piloted control of this degree of freedom may not present any significant difficulties. This is consistent with the characteristics of conventional blimps which, owing to their well behaved roll characteristics, do not employ active control over this degree of freedom. However, since the payload cable attach point is located 55 ft below the roll instantaneous center of rotation, significant coupling between payload cable hook motions and gust and/or lateral control inputs should be expected. As in the pitch mode, this may be troublesome during load pickup operations. An active cable control system may be desirable to restrict such undesirable coupling characteristics with the pitch and roll motions (Ref. 6).

The vehicle/slung load configuration has 11 characteristic modes of response. The first five of these, corresponding to the basic vehicle modes discussed above, induce significant payload motion. The damping of the vehicle heave mode increases slightly due to the increased rotor

loading ($1/T_h = 0.1092$ rad/sec) and induces in-phase equal-magnitude (i.e., rigid body) motion of the payload ($w_h = w_p$). The increase in the heave mode frequency also occurs for the maximum vehicle weight configuration ($1/T_h = 0.1006$ rad/sec), as expected.

The maximum weight and slung-payload configurations exhibit an unstable surge subsidence mode ($1/T_s = -0.0009$ rad/sec). The source of this instability can be explained from the following approximate expression,

$$1/T_s \doteq -X_u + \frac{M_u X_\theta}{M_\theta} \quad (8)$$

where

X_u Axial force derivative with respect to speed; i.e. axial drag damping

M_u Pitching moment derivative with respect to speed; i.e. attitude/speed coupling derivative

X_θ Axial force due derivative with respect to pitch attitude
 $(= \frac{B - W}{m e_z})$

M_θ Pitching moment derivative with respect to pitch attitude, i.e., pitch attitude stiffness

The drag damping derivative (X_u) is always negative (stable) resulting from axial drag, rotor flapping, and propeller damping. Since the rotor thrust line is below the vehicle c.g., rotor flapping causes a negative (unstable) value of the pitching moment derivative (M_u). The pitch attitude derivatives (X_θ and M_θ) result from buoyancy and metacentric height effects and are negative for all flight speeds. When the rotors are lightly loaded (nominal and minimum weight configurations), M_u is negligible and the surge mode is stable,

$$\frac{1}{T_s} \doteq -X_u \quad (9)$$

However, for higher rotor thrust levels (maximum weight and slung load configurations), the associated increased rotor flapping yields greater negative values of M_u , which destabilizes the surge mode (Eq. 8). The eigenvectors associated with the vehicle/slung-load coupled surge mode display in-phase (rigid body) motions of the hull and payload as before. Unwanted remnants in axial velocities due to the unstable surge mode characteristics will therefore be propagated to the payload and contribute to the problems of precision stationkeeping and payload positioning.

The addition of the slung payload causes a significant stabilization of the pitch oscillation mode in comparison with the unloaded vehicle. The improved damping ratio ($\zeta_p = 0.25$) results from higher rotor trim thrust levels (increased pitch damping) and the out-of-phase motions of the payload (Fig. 8). The eigenvector results of Fig. 8 indicate a reduction in pitching motion relative to axial translation in the pitching oscillation mode.

$$|\theta_h : x_{hcg}|_{\omega_p} = |0.270 : 1_{ft}|$$

The well damped characteristics of the coupled pitch oscillation mode suggest that there will be no special problems associated with the manual control of the vehicle pitch attitude in this flight condition.

As in the pitch mode, the addition of the slung payload causes an improvement in the roll oscillation characteristics ($\zeta_r = 0.252$, $\omega_r = 0.602$ rad/sec). The increased damping ratio is largely due to the increased rotor damping with only a small contribution from coupled payload motion. In this case, the payload and hull attitude variations are roughly equal in magnitude and phase ($\phi_p \approx \phi_h$, in Fig. 9), indicating that the payload is acting as a rigid body extension of the vehicle roll mode. Therefore, manual control of the vehicle roll attitude should not present any special difficulties in this flight condition.

The yaw sway modes ($1/T_{sy1}$, $1/T_{sy2}$) for the vehicle slung-load configuration have improved damping characteristics owing to the increased level of rotor trim thrust and associated damping due to rotor flapping, $1/T_{sy1} = 0.0176$, $1/T_{sy2} = 0.0222$ rad/sec.

ORIGINAL PAGE 19
OF POOR QUALITY

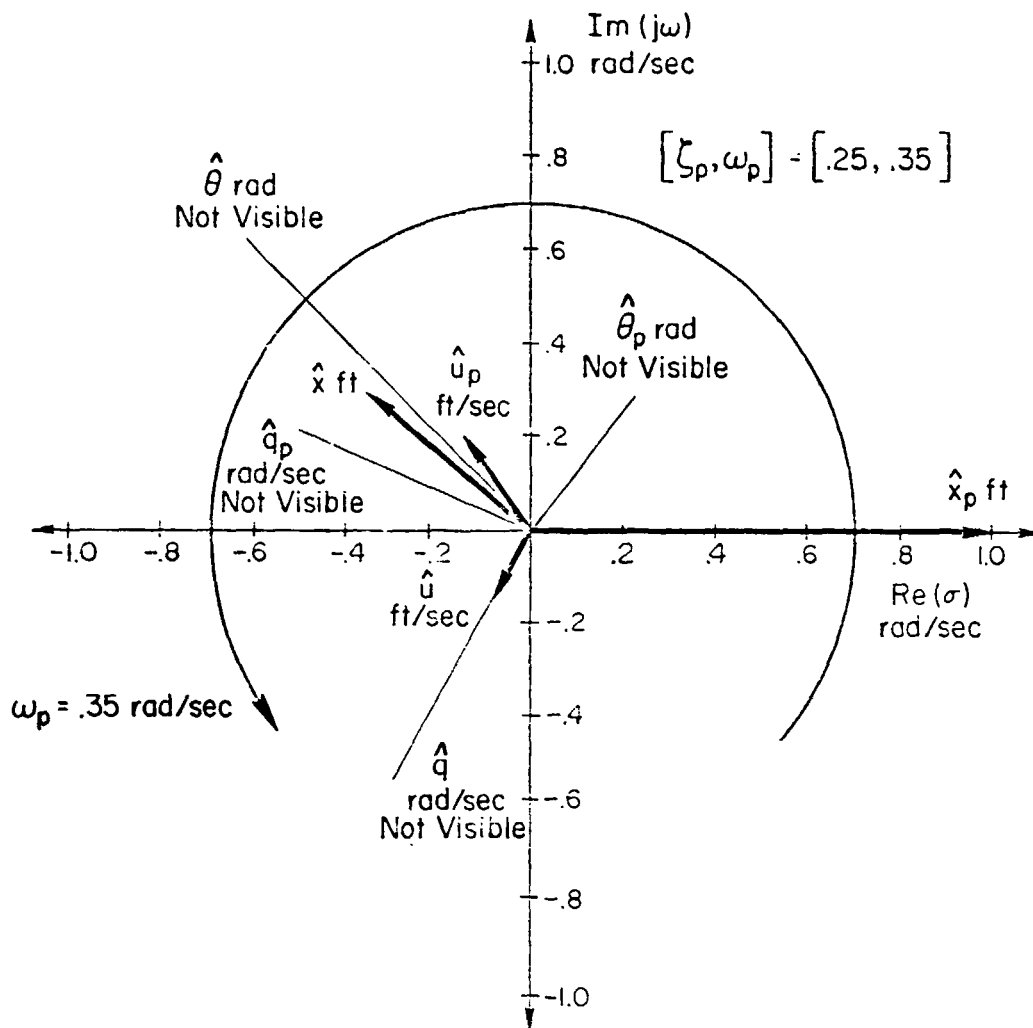


Figure 8. Pitch Mode, Vehicle/Slung-Load Configuration; $V_a = 0$

ORIGINAL PAGE IS
OF POOR QUALITY

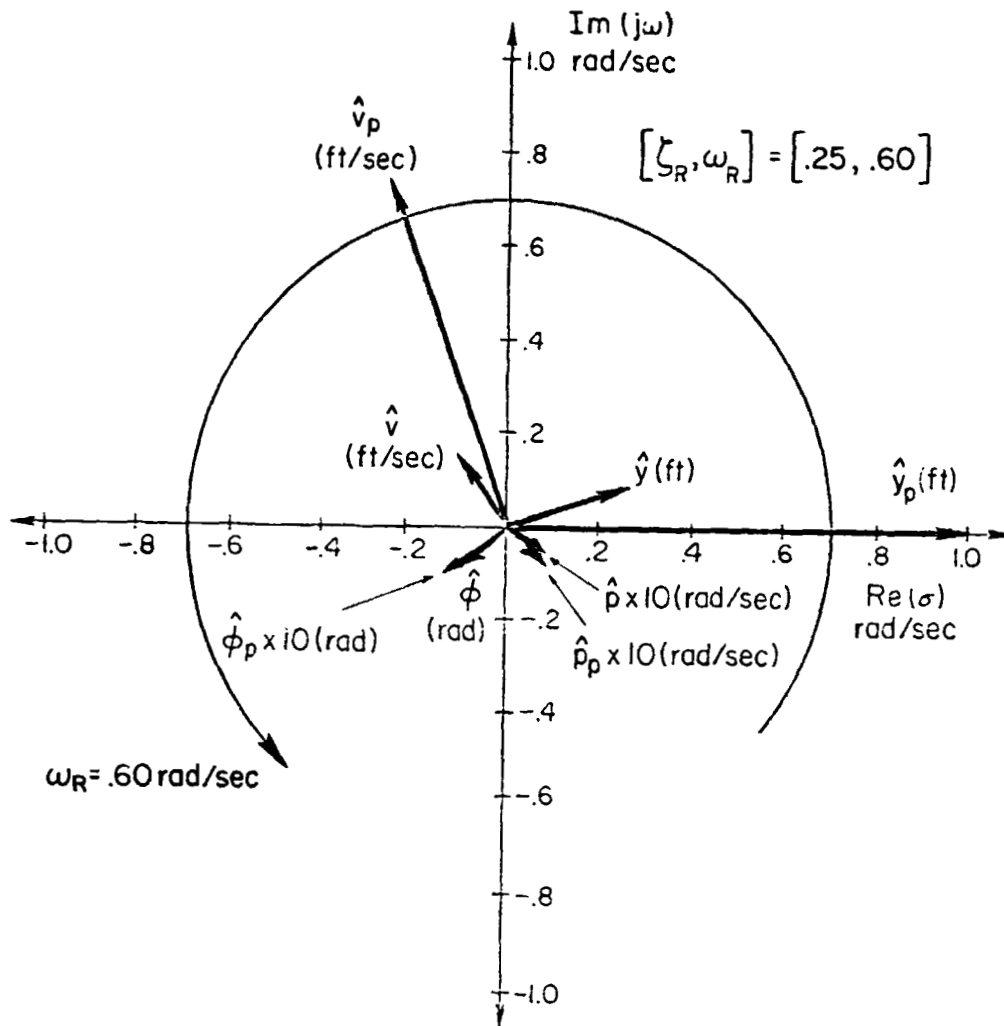


Figure 9. Roll Mode, Vehicle/Slung-Load Configuration; $V_a = 0$

In addition to the five basic vehicle modes (12 eigenvalues), there are an additional six modes of response associated with the slung-load system in isolation:

- 1) Yaw vibration ($\zeta_{y_v}, \omega_{y_v}$)
- 2) Longitudinal pendulum ($\zeta_{lon}, \omega_{lon}$)
- 3) Lateral pendulum ($\zeta_{lat}, \omega_{lat}$)
- 4) Pitch vibration ($\zeta_{p_v}, \omega_{p_v}$)
- 5) Roll vibration ($\zeta_{r_v}, \omega_{r_v}$)
- 6) Heave vibration ($\zeta_{h_v}, \omega_{h_v}$)

The lowest frequency mode ($\zeta_{y_v}, \omega_{y_v}$) is associated with the yawing motion of the payload about an axis colinear with the cable. Since the yaw inertia and cable angular spring constants are both very low, this motion is undamped with a very low natural frequency ($\omega_{y_v} = 0.0132$ rad/sec) and does not induce any motions of the hull. The yaw vibration mode can be ignored for the present payload/cable configuration.

The next two lowest frequency modes are associated with the longitudinal ($\zeta_{lon}, \omega_{lon}$) and the lateral ($\zeta_{lat}, \omega_{lat}$) payload pendulum modes. The eigenvector diagram for the pitch pendulum mode (ω_{lon}) is shown in Fig. 10. The motions of the payload and the hull are roughly 90 degrees out-of-phase and the instantaneous-center-of-unforced pitch motion is located just below the cable attach point on the hull. The payload lateral pendulum mode, ω_{lat} is directly analogous to the longitudinal pendulum mode, with the instantaneous center of rotation at approximately the same location. The modal frequencies ($\omega_{lon}, \omega_{lat}$) are governed by the length of the cable ($l = 250$ ft) and the distance from the cable attach point to the payload c.g. ($z_\ell = 12.6$ ft),

$$\omega_{lon} \doteq \omega_{lat} \doteq \sqrt{\frac{g}{l + z_\ell}} = 0.350 \text{ rad/sec} \quad (10)$$

which shows that payload pendulum frequencies are very close to the vehicle pitch and roll oscillation frequencies. Since the payload

ORIGINAL PAGE IS
OF POOR QUALITY

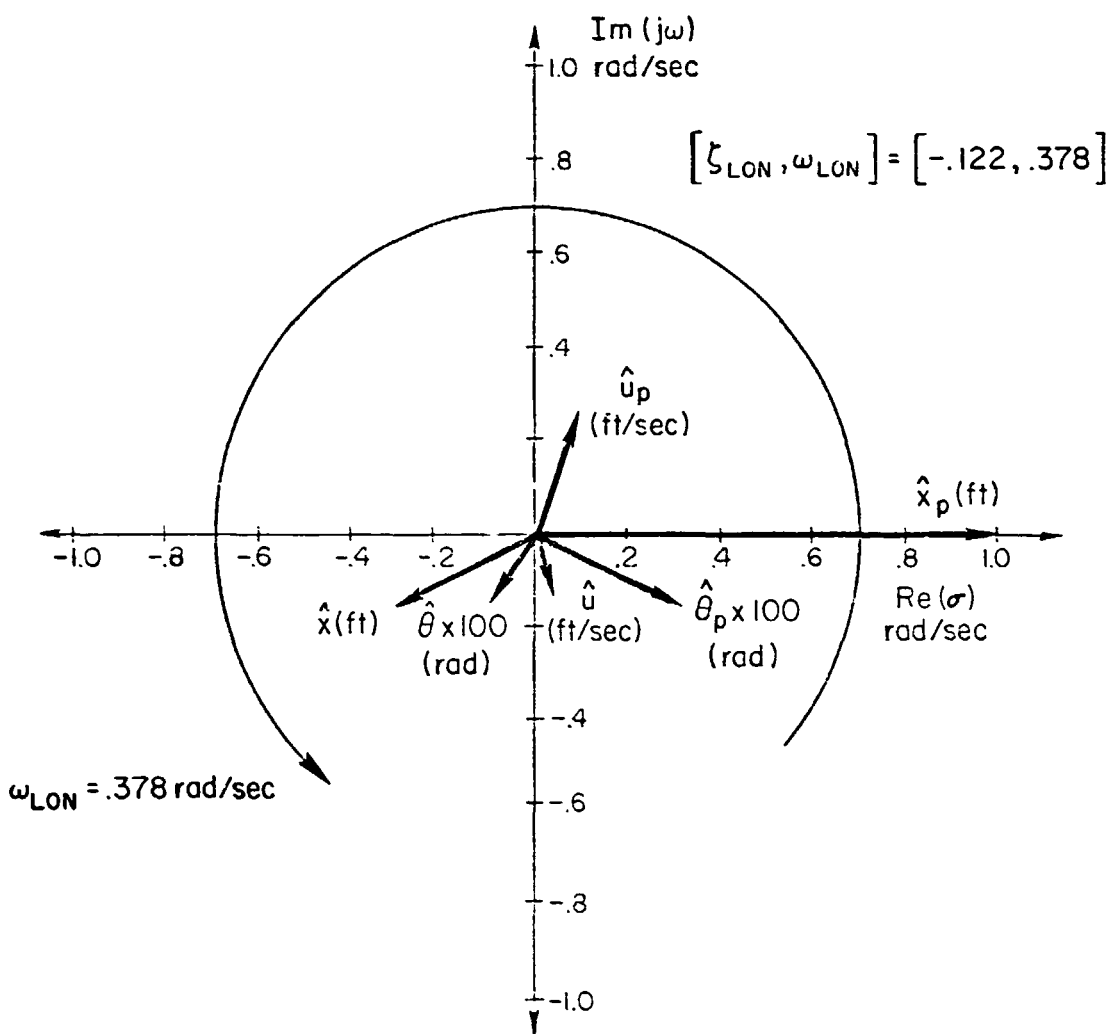


Figure 10. Pitch Pendulum Mode; $V_a = 0$

pendulum motion is poorly damped in hover ($\zeta_{lon} \doteq \zeta_{lat} \doteq 0$), it will be excited by gust and control inputs to the vehicle, causing positioning problems typical in helicopter operations (Refs. 6, 8).

The next two frequency modes (ω_{p_v} , ω_{r_v}) are associated with the angular vibratory motion of the payload about the cable attach point, due to its offset from the payload center of gravity. These modes are marginally stable with roughly equal natural frequencies of 1.7 rad/sec. Their characteristics are governed by the mass of the payload, the spring constant of the cable and the distance between the payload center-of-gravity and the cable attach point on the hull ($l + z_l$). The motions of the vehicle and payload are 180 deg out of phase. In both modes the induced hull linear motion is about 25 percent of the payload linear motion and the large frequency separation between the two systems precludes stationkeeping-related implications. However, the poor damping characteristics of these modes will result in large payload oscillations, hampering load positioning tasks.

The highest frequency mode ($\zeta_{h_v} = 0.787$, $\omega_{h_v} = 11.45$ rad/sec) is associated with the vibratory heave motion of the payload cable. This mode is heavily damped due to the assumed cable characteristics. As before, the motion of the payload and hull are 180 degree out-of-phase. The magnitude ratio is inversely proportional to the ratio of payload mass to effective vehicle mass for z-axis motions,

$$\left| \frac{w_{h.c.g.}}{w_{p.c.g.}} \right|_{\omega_{h_v}} = |0.224:1| \doteq \frac{\text{Payload Mass}}{\text{Effective Vehicle Mass for z-axis Motions}} = 0.221$$

The relatively high frequency, out-of-phase, vibrating modes (ω_{p_v} , ω_{r_v} , ω_{h_v}), although not important for low frequency stationkeeping tasks, may excite vehicle modes associated with the structural dynamics of the interconnecting frame and control system. Also, rotor excitation including higher order dynamics not modeled in the present simulation could be significant at these frequencies ($\Omega_{rotor} \doteq 3.5\omega_{h_v}$).

B. EFFECT OF AXIAL SPEED ON DYNAMICS CHARACTERISTICS

As the forward flight speed of the vehicle is increased, the rotors become more effective and their contribution to the vehicle damping increases. This results in increased frequency (reduced time constants) of the surge, $(1/T_s)$ heave, (i/T_h) and sway $(1/T_{sy2})$ modes as shown in Fig. 11 for the nominal configuration. Note that the sway and heave modes are roughly at the same frequency, since the vehicle drag and effective mass characteristics which dominate the higher speed properties are nearly equal in the lateral and vertical directions.

The yaw mode is governed by the unstable yawing moment characteristics of the hull/tail assembly which become increasingly important as their contribution grows with the square of the forward flight speed. Since there is no metacentric stability in yaw, the yaw mode $(1/T_{sy1})$ becomes unstable for all forward (and rearward speeds) as shown in Fig. 12. Uncorrected disturbances of this mode will cause the vehicle to increase its sideslip angle until the stable orientation of $\beta = 78.8$ deg is reached (Fig. 6). For the unloaded vehicle cruise speed of 50 kts, the time-to-double amplitude is 2 sec, suggesting a highly unstable configuration. Also shown on the figure are the results for the vehicle/slung payload configuration, from which we notice very little change in the characteristics of this mode with rotor loading. This result is expected since the sideslip characteristics at high forward flight speeds are almost entirely dominated by the hull and tail aerodynamics.

The dynamics of the vehicle pitch oscillation mode in forward flight may be approximated by a 2 DOF model involving pitch and heave motions. Expansion of the 2 DOF characteristic equation yields the following requirement for the pitch oscillation mode to be dynamically stable

$$-M_{\theta} + M_q Z_w - M_w Z_q > 0 \quad (11)$$

The first term in Eq. 11, the metacentric stability, is independent of flight speed. The second term, which is a product of the pitch and

ORIGINAL PAGE 9
OF POOR QUALITY

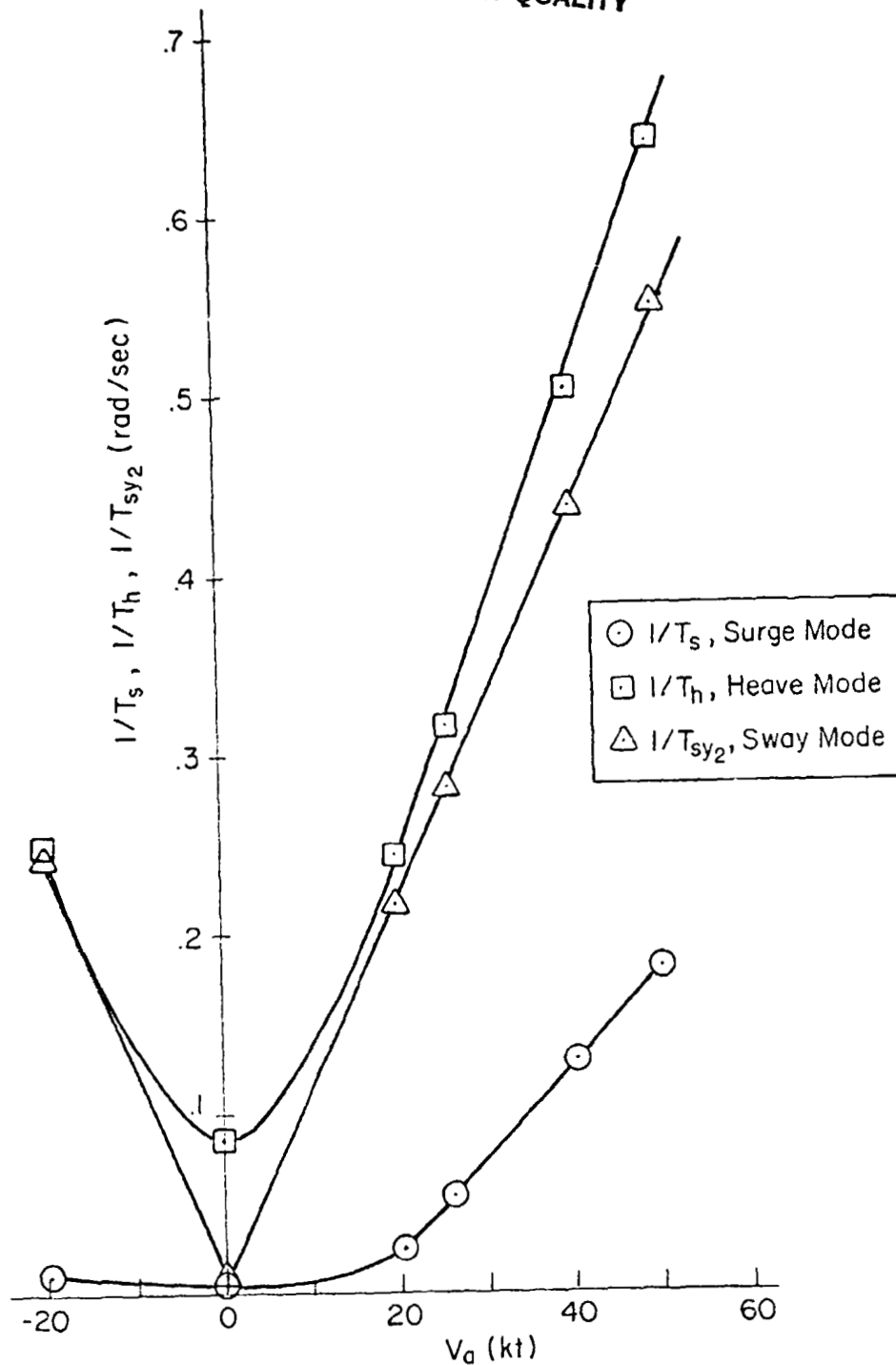


Figure 11. Variation of Surge ($1/T_s$), Heave ($1/T_h$), and Sway ($1/T_{sy2}$) Modes with Axial Speed; Nominal Configuration

ORIGINAL PAGE IS
OF POOR QUALITY

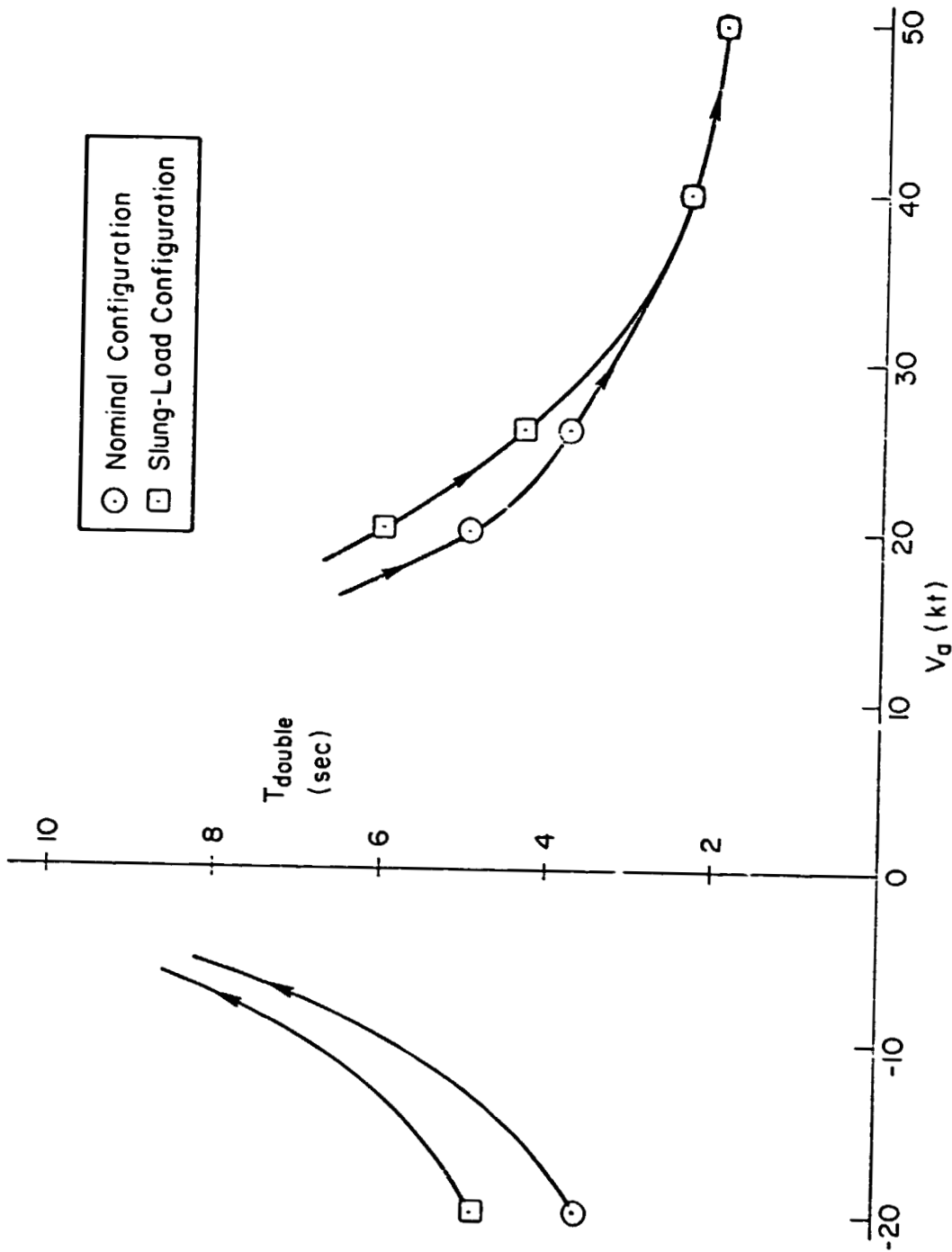


Figure 12. Effect of Axial Airspeed on Yaw Instability, $1/T_{sy1}$, for the Nominal and Slung-Load Configurations

heave damping, increases with speed due to the improving effectiveness of the rotors as damping devices. The third term is the aerodynamic instability contribution which grows rapidly with increasing speed. For high forward speeds, this term overcomes the stabilizing influence of the first two terms ultimately destabilizing the vehicle pitch mode.

The migration of the pitch oscillation roots with increasing flight speed is shown in Fig. 13. As previously noted, when the roots have positive real parts (left half of s-plane) the pitch oscillations are stable and die out with time. However, when the roots are in the right half plane with associated real parts having positive values, the oscillations are unstable and grow with time. The stability/instability boundary is the imaginary ($j\omega$) axis. The roots of the unloaded nominal vehicle cross this boundary when the airspeed is equal to 35 kts. The corresponding results for vehicle/slung-payload configuration show the onset of instability to occur at roughly the same airspeed.

In the nominal cruise configuration (50 kts, unloaded), the time-to-double amplitude is 8.7 sec. For the loaded configuration, the time-to-double amplitude in the cruise condition (40 kts) is 17.3 sec. As before, these results indicate that the unloaded configuration remains the critical case for piloted handling qualities. As will be shown later, manual control of attitude and translation loops will allow the pilot to stabilize these otherwise unstable modes at the expense of degraded pilot opinion of the vehicle's handling qualities. However, the location of the roots indicate the severe instability of the vehicle in unattended operation.

The stabilization of the payload longitudinal pendulum oscillation mode (ω_{lon}) with increasing airspeed is also shown in Fig. 13. This is due to the increase in the payload drag damping,

$$X_{up} = (\rho S_p C_{Dp}) u_{trim} \quad (12)$$

The payload lateral pendulum oscillation mode (ω_{lat}) is not affected by axial airspeed ($v_{trim} = 0$), so payload lateral oscillations will persist at cruise flight conditions

ORIGINAL PAGE IS
OF POOR QUALITY

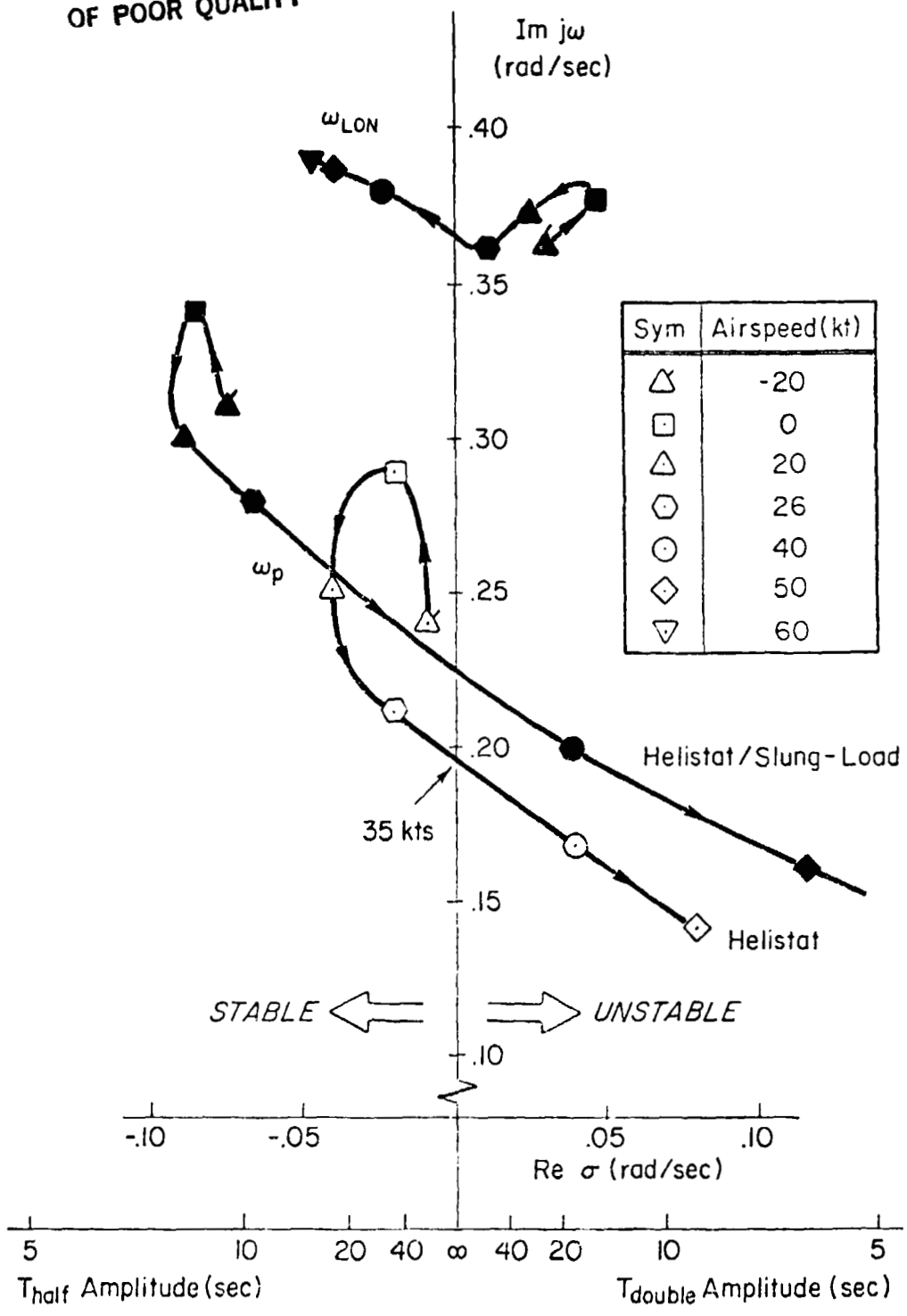


Figure 13. Migration of the Pitch Oscillation Mode of the Vehicle (ω_p) and Payload (ω_{LON}) with Axial Airspeed

C. EFFECT OF SIDESLIP ON DYNAMICS CHARACTERISTICS

Since it is unlikely that the vehicle will always operate in a zero or 90 deg sideslip condition, the effect of varying sideslip on the vehicle dynamics was investigated. The flight condition for this study was hover with a 15 kt wind of varying sideslip angle. This condition is typical of the expected operating environment of the Helistat.

Increased sideslip has a favorable effect on all the modes of vehicle response, with the exception of the roll oscillation mode. The migration of the roll oscillation roots with varying sideslip angle is shown in Fig. 14. While for most angles of sideslip the roll mode is not significantly effected, there is a strong sensitivity of the results in the 60-120 deg sideslip range.

The source of this sensitivity is in the relative loading of the rotors. For most angles of sideslip, all of the rotors maintain at significant levels of positive or negative rotor thrust. However, in the nominal case the upwind rotors (2 and 4) show a significant reduction in thrust levels for the 60^o-120^o sideslip cases due to the specific associated roll angle requirements. This symmetric reduction in the rotor thrust levels on the upwind side greatly reduces the roll damping of the vehicle.

In the 45 deg sideslip case, the roll damping derivative is $L_p = -0.279$ and the roll oscillation damping ratio is $\zeta_r = 0.27$. However, when the sideslip angle is increased to 60 deg, the very low thrust levels of the upwind rotors causes an associated reduction in roll damping, $L_p = -0.096$, yielding a roll oscillation damping ratio of $\zeta_p = 0.013$. When the sideslip angle is increased to 90 deg the upwind rotors have significant negative thrust due to inflow of the ambient wind through the top of the rotor (even for small positive values of collective pitch) and the roll damping reaches a maximum stable value, $L_p = -0.351$ yielding a damping ratio of $\zeta_r = 0.383$. At a 120 deg sideslip angle, the upwind rotors are again unloaded, resulting in reduced roll damping, $L_p = -0.100$ and associated damping ratio, $\zeta_r = 0.034$. Similar

ORIGINAL PAGE 13
OF POOR QUALITY

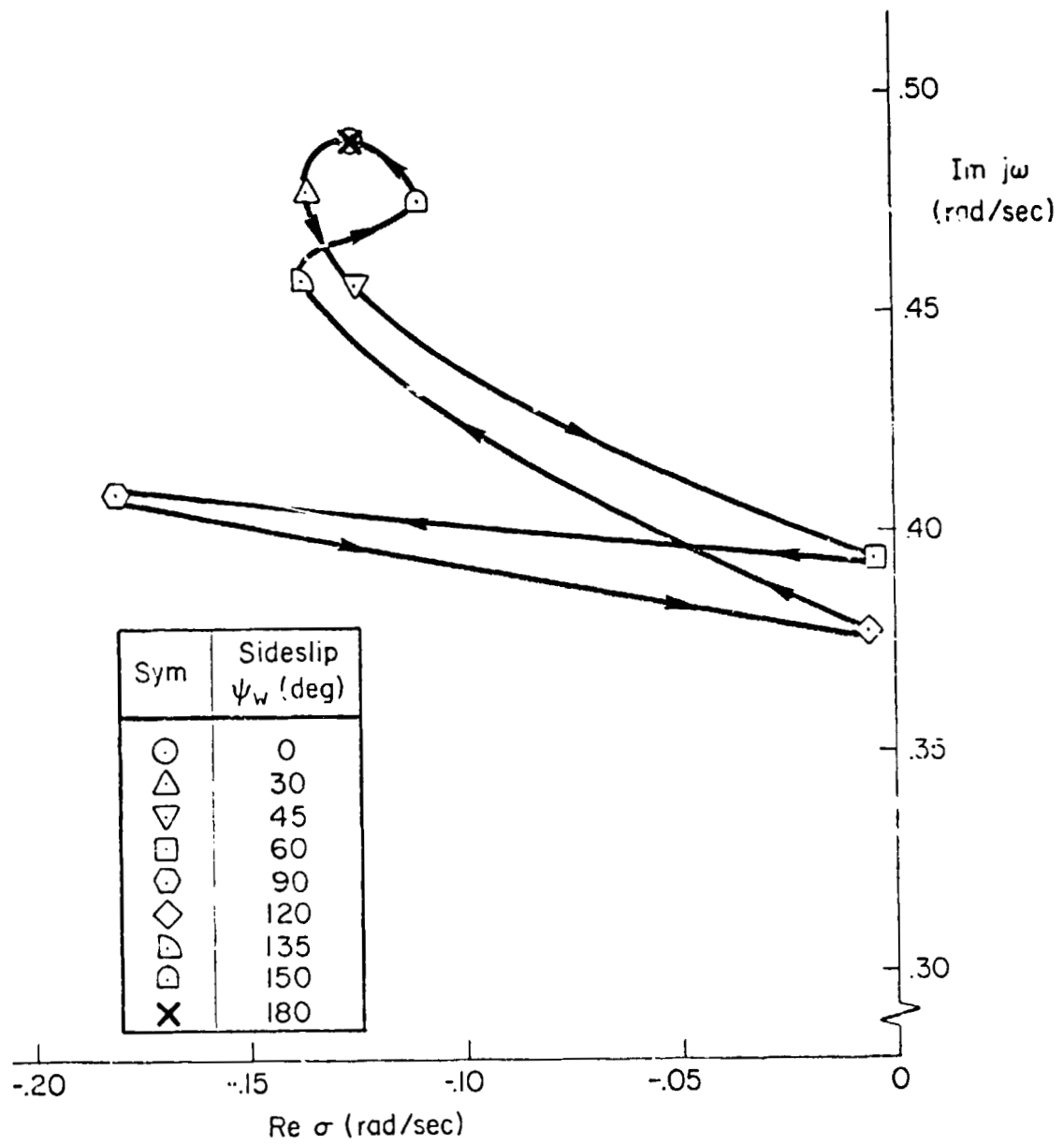


Figure 14. Migration of Roll Oscillation Mode (ζ_R, ω_R) with Sideslip; Nominal Configuration; $V_w = 15$ kt

sideslip sensitivities were found to occur for both the minimum weight and maximum weight vehicles with slight changes in the critical sideslip angles. Strong sideslip sensitivities were not apparent in the case of the vehicle with the slung payload because high rotor thrust levels and associated small trim roll angles resulted in more balanced rotor loading conditions.

These results show that significant reductions in the roll damping of the vehicle result when the rotors are unloaded. As discussed in the next section, the analogous effect on pitch oscillation dynamics results from an aft shift in the vehicle c.g. location causing the forward rotors to become unloaded. The combination of degraded roll dynamics and reduced control margins (Fig. 6) makes the large sideslip angle regime a critical flight-regime for the unloaded vehicle. It is clear that such conditions should be avoided if possible.

D. FOUR-FINNED CONFIGURATION

Analysis of the vehicle dynamics and handling qualities for a 4-finned (X) configuration assumed that adjustments in the ballast and ballonets would be made to maintain constant mass and center of gravity characteristics. The aerodynamic force and moment contributions of the extra surfaces are greater than those which would be obtained by simply doubling the coefficients of the first two fins (Ref. 9, 10).

The major effect of adding the two additional fins is an improvement in the pitch and yaw stability of the vehicle. Figure 15 shows the variation of the unstable yaw mode ($1/T_{SY1}$) with increasing flight speed for the 4-finned configuration. Significant improvement in the dynamic characteristics are achieved over the entire speed range (compare Fig. 15 vs. Fig. 12). At the cruise speed of 50 kts, the time to double amplitude is increased from 2 sec to 7 sec. Similar improvements are shown in Fig. 15 for the vehicle/slung-load configuration. Once again the loading effects become less significant at higher flight speeds.

The reduction in the aerodynamic instability term, ($M_w Z_q$) of Eq. 11, causes a delay in the onset of pitch instability as shown in Fig. 16.

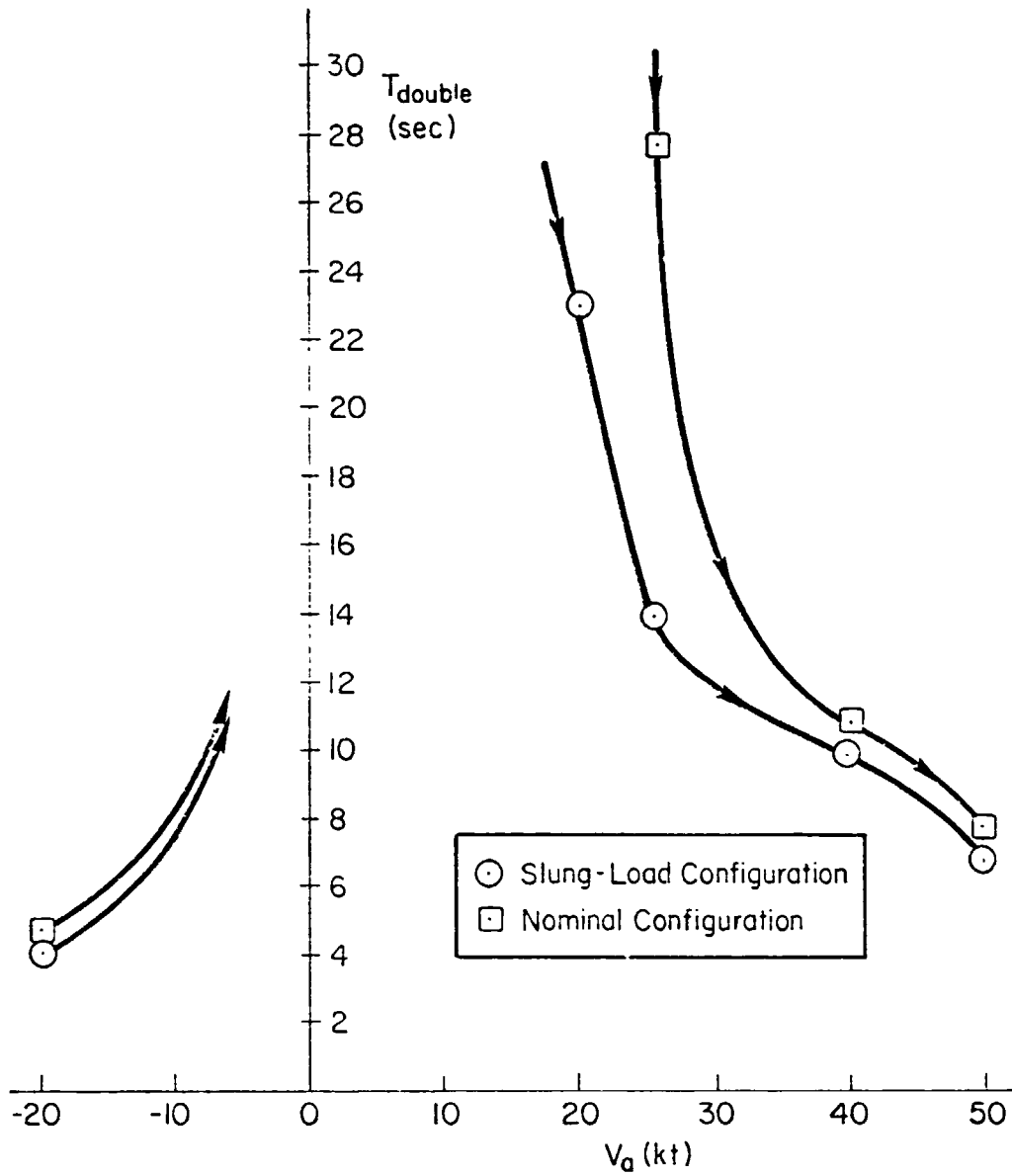


Figure 15. Effect of Axial Airspeed on Yaw Instability, $1/T_{sy1}$, 4-FINS

ORIGINAL PAGE 13
OF POOR QUALITY

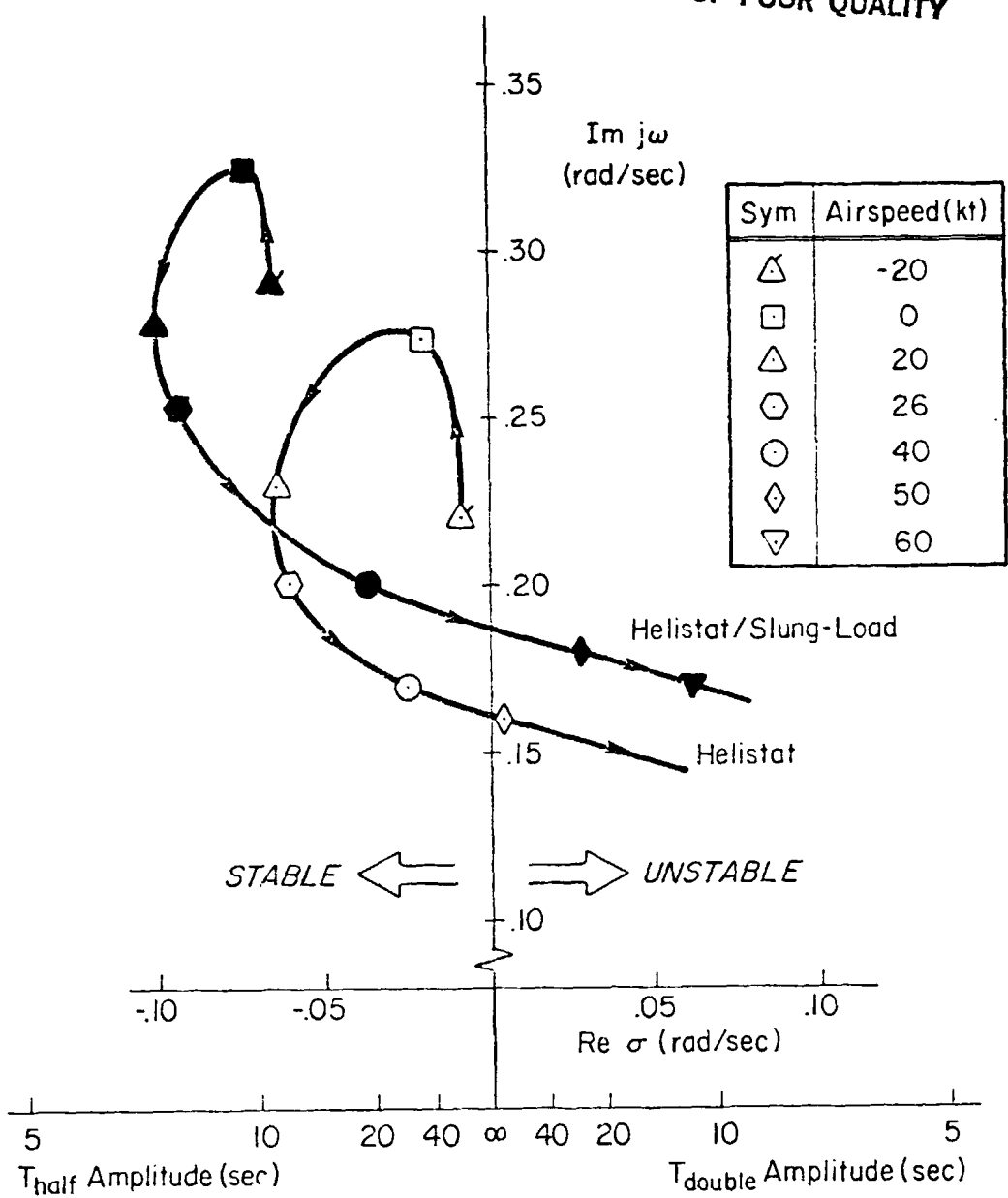


Figure 16. Migration of the Pitch Oscillation Mode (ω_p) with Axial Airspeed, 4-FINS



For the cruise speed of 50 kts, the 4-finned configuration is neutrally stable. Similar improvements are shown for the vehicle/slung payload configuration which exhibits a stable pitch oscillation mode for the cruise speed of 40 kts (time-to-half amplitude = 17 sec). These lightly damped (and marginally unstable) dynamic characteristics of the 4-finned configuration are typical of operational blimps, which tend to "wander" around the nominal course. A 3-finned, inverted-Y configuration with higher aspect ratio surfaces would further improve the cruise stability characteristics beyond those of the original 4-finned airship (ZPG-2).

The 4-fin configuration analysis discussed above was repeated with an adjustment in the mass and c.g. characteristics to account for the additional weight of the two extra fin surfaces if the ballast and ballonets are not retrimmed. The new hull c.g. is located 4.7 ft aft of the nominal position, resulting in a large nose-down pitch control adjustment to maintain vehicle trim in cruise. Uneven thrust levels on the fore and aft rotors caused major changes in the stability derivatives of Eq. 11 for the 50 kt cruise condition. Compared to the 4-finned configuration with nominal mass and c.g. characteristics, the aft c.g. configuration exhibits a 44 percent reduction in the pitch stability term, $M_q Z_w$ and a 47 percent increase in the pitch instability term $M_w Z_q$. The resulting aft c.g. pitch mode is $(\zeta_p, \omega_p) = (-0.540, 0.16)$ compared to $(\zeta_p, \omega_p) = (-0.022, 0.162)$ for the nominal c.g., with associated times-to-double amplitudes of 8.039 sec and 198.0 sec, respectively. Therefore, any changes in the tail configuration need to be balanced by associated retrim of the ballonets and/or ballasting of the vehicle in order to maintain the nominal c.g. location.

The strong sensitivity of the pitch (and roll) characteristics of the vehicle with rotor loading suggests the need for c.g. travel guidelines for the operational vehicle. Some alleviation of the sensitivity to c.g. location could be obtained by increasing the usage of the aerodynamic tail surfaces in order to relieve uneven rotor thrust levels required for pitch and roll trim control. However, c.g. restrictions for hover would still be necessary.

**A FOOTNOTE ON THE COMPARISON OF HELISTAT DYNAMICS
WITH VSTOL HANDLING QUALITY SPECIFICATIONS**

Any attempt to specify desired handling qualities for the Helistat must be couched in terms of the operational requirements and objectives of the vehicle. For example, while the Helistat must achieve and maintain precision stationkeeping, it would be unreasonable to expect performance to equal that of a standard helicopter. Conversely, the dynamics specifications of typical hovering VSTOL's need to be fairly severe since such vehicles can become control limited very rapidly, with resulting loss of lift and catastrophic consequences. The Helistat on the other hand, with its near neutral buoyancy condition, need not be as severely restricted since the buoyancy of the vehicle provides a significant percentage of the vertical equilibrium condition. As such, concerns over spiral instability and catastrophic loss of control is not as significant for the Helistat in the hovering environment.

Handling qualities specifications for the Helistat in cruise have analogous implications. Unlike military aircraft, there is no requirement for LTA vehicles to maintain precision flight path control in cruise; so, it is common for operational blimps to "wander" around the nominal course. This is a design tradeoff between lateral stability for adequate cruise handling qualities and the weight penalty associated with increased tail area.

In summary, while it is useful to make comparisons between the dynamics of Helistat and other VSTOL aircraft it is not possible to draw specific conclusions on the handling qualities of the vehicle until a more complete analysis of the manual control problem is completed. This will be the primary subject of the remaining analysis effort.

SECTION VI

NONLINEAR RESPONSE TO CONTROL

The nonlinear response of the nominal configuration to a lateral stick input was calculated to illustrate the roll-to-translate control characteristics and to compare nonlinear time histories with the previous linearized results. The unloaded vehicle was trimmed in the hover flight condition and subjected to a lateral control input of 0.1 rad, the maximum input before surface limiting occurs. So, the steady state condition corresponds to the maximum unloaded crosswind results of Fig. 5.

Figure 17 shows that the nonlinear roll angle response is dominated by the damped second-order roll oscillation mode (ω_r), with the time-to-maximum amplitude well approximated by the linear solution,

$$t_{\max} = \frac{\pi}{\omega_r \sqrt{1 - \zeta_r^2}} \quad (13)$$

The steady-state roll angle is about 40 degrees, as expected from Fig. 5. The maximum overshoot ($\phi_{\max}/\phi_{\text{steady state}} = 2.06$) is 30 percent larger than the linear solution,

$$\frac{\phi_{\max}}{\phi_{\text{steady state}}} = 1 + e^{-\pi \zeta_r / \sqrt{1 - \zeta_r^2}} = 1.59 \quad (14)$$

due to nonlinearities in the vehicle kinematics and dynamics. The yaw angle response (ψ) is slow and first order due to the long dominant time constants, T_{sy1} and T_{sy2} . The maximum total lateral acceleration ($\sqrt{a_y^2 + a_z^2}$) is 0.13 g's, with a steady-state lateral velocity of about 15 kts. This steady-state velocity is consistent with the 40 degree steady-state roll angle shown in Fig. 5. These results show the utility of the linearized models, but suggest the existence of important nonlinearities during gross maneuvers. As discussed earlier, the structural and handling quality implications associated with these large (rigid body) roll angle transients ($\phi_{\max} = 82.4$ deg) will be very important in the operational environment.

ORIGINAL PAGE IS
OF POOR QUALITY

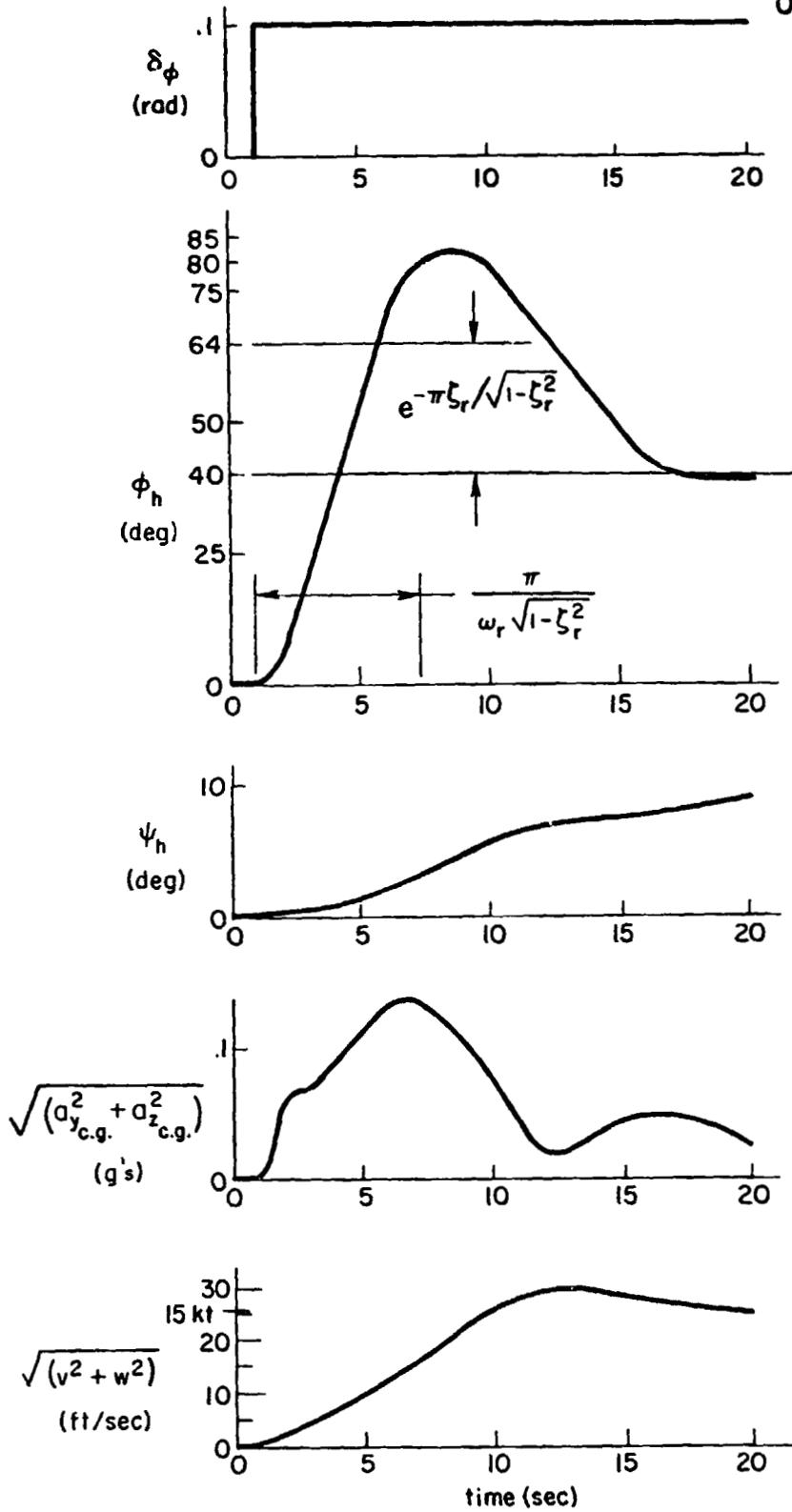


Figure 17. Response to Lateral Control Input, $\delta_\phi = 0.1$ rad
 $V_a = 0$, Nominal Configuration

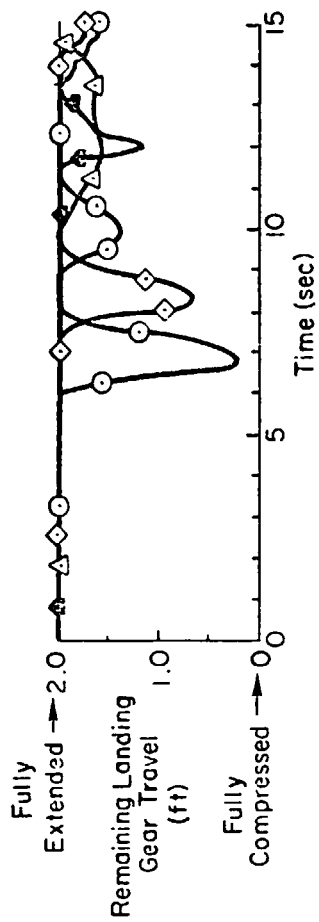
SECTION VII

LANDING CHARACTERISTICS

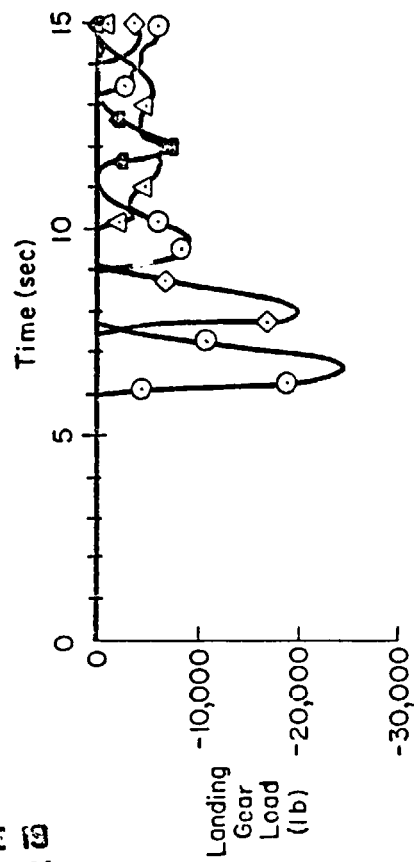
The landing gear and support structure on the Helistat is designed to withstand impact loads resulting from vertical landing velocities of 5 ft/sec with the contact on a single wheel (Ref. 11). In addition, the pilot is assumed to reduce the trim thrust level 33 percent at the time of ground impact to avoid rebounding after the first compression cycle. To simulate this condition, the vehicle is trimmed for a 5 ft/sec descent rate at an attitude of 5 deg nose up and 5 deg right roll. This insures that the rear right landing gear (No. 4) will absorb all of the initial landing impact. When the wheel just touches the ground, the rotor thrust levels are reduced by 36 percent, as shown in Fig. 18.

The initial compression of landing gear 4 is 86.9 percent of its available travel with a remaining extension of 0.272 ft. The maximum landing gear load of 24,444 lb compression is developed 0.5 sec after impact. This asymmetrical load causes the vehicle to pitch down and roll left, resulting in ground contact of landing gear 3 (rear left landing gear). Due to the reduced kinetic energy of the system following the initial impact, landing gear 3 compresses 70 percent of the available travel with a maximum force of 20,600 lbs. The vehicle continues to pitch and roll with decreasing amplitude, nearing a steady state condition after 10 sec following initial impact.

These results show that the landing gear configuration meets current design specifications for a 5,000 ft base altitude. However, additional travel and/or spring stiffness may be desired to increase the safety margin for this weight condition. Since the maximum landing weight for sea level based operations is only 2.7 percent higher than the current (5,000 ft based) level, altitude effects on these results will not be significant.



ORIGINAL PAGE IS
OF POOR QUALITY



Note: The symbols are for identification purposes only.

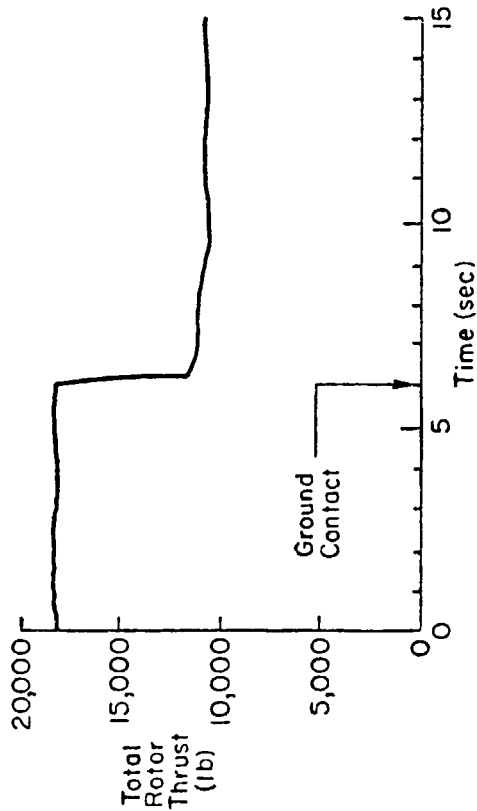
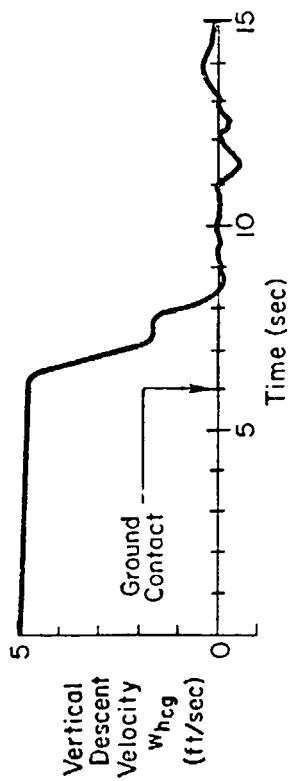


Figure 14. Simulation of Landing Dynamics; 5,000 ft Based Operations

SECTION VIII

MOORING CHARACTERISTICS

The mooring response of the vehicle was calculated for ambient wind conditions of 15 kts and 60 kts. The standard mooring weight of 78,245 lb was used, which is based on ballonet settings for 1000 ft pressure altitude (AGL) operations, 10 percent fuel and no payload. This yields a buoyancy ratio of 0.82 for the base operations site of 5000 ft above sea level.

The non-linear mooring simulation assumes that the vehicle is attached to the mooring mast by a free nose gimbal which allows 3 degrees-of-angular freedom and no linear freedom. For the present four landing gear configuration the moored vehicle exhibits four basic modes of motion. The lowest frequency mode is a first order 1 DOF yawing motion ($1/T_y$). The modal frequency is determined by the inertial characteristics of the vehicle, the wind speed, and the tail configuration. For the 15 kt case, $1/T_y = 0.0767$ rad/sec, increasing to $1/T_y = 0.1710$ rad/sec for the 60 kt case.

The next highest frequency mode (ω_{y_v}) involves significant yawing and rolling motions of the hull, alternately compressing the left and right landing gears. This mode also depends on the inertial and geometric characteristics of the vehicle and wind speed; and on additionally important parameters of the landing gear's spring stiffness and damping. The damping ratio and frequency are $\zeta_{y_v} = 0.540$ and $\omega_{y_v} = 1.189$ rad/sec for the 15 kt condition, increasing to $\zeta_{y_v} = 0.824$ and $\omega_{y_v} = 3.002$ rad/sec for the 60 kt condition. The next mode is associated with the oscillatory pitching motion of the vehicle about the mast and is dominated by the vehicle mass properties and landing gear characteristics. This mode is unaffected by the ambient wind speed, having a constant damping ratio and natural frequency of $\zeta_{p_v} = 0.47$ and $\omega_{p_v} = 2.7$ rad/sec, respectively.

In the 15 kt case, the highest frequency mode, $1/T_{r_v}$, is associated with the 1 DOF rolling motion of the vehicle about the mooring point. The time constant is controlled by the inertial characteristics of the vehicle, the landing gear spring characteristics, and the ambient wind speed. When the wind speed is increased to 60 kts the predominant motion variable is yawing velocity with a major component of rolling velocity still present. The modal frequency of the 60 kt case is $1/T_{r_v} = 4.117$ rad/sec compared to $1/T_{r_v} = 9.522$ rad/sec for the 15 kt case. The changes in the dynamic characteristics of this mode are due to the increased aerodynamic damping of the hull at the high wind speeds.

The time history response of the moored vehicle to a (1 - cosine) lateral gust is shown in Fig. 19. The maximum amplitude of the disturbance is 27 ft/sec, or 27 percent of the mean wind. This can be considered as a 2σ gust with a 1σ value of 13.5 percent of the mean wind, a typical level for moderate turbulence conditions (Ref. 12). As shown in Fig. 19, the lateral gust causes the vehicle to initially roll to the left and then to the right with a maximum amplitude of 1.7 deg. The maximum yaw angle of 4.4 deg occurs at 3.75 sec elapsed time. It is interesting to note that the vehicle does not return to the zero sideslip angle but is rather approaching a second more stable yaw angle at a slight offset to the zero sideslip condition. During the transient, the vehicle sustains a maximum lateral nose cone force of 20,500 lbs and a maximum axial load of 22,682 lbs. The existing operational limits are based on quasi-steady calculations (Ref. 13) which do not properly account for the large gust acceleration and gust gradient effects (Ref. 1). These limits need to be re-evaluated to reflect the present results.

The preceding analysis was repeated for the 4-fin configuration. The additional weathercock stability reduced the maximum yaw angle displacement to 4.05 deg, with negligible changes in the other motion variables. Since the applied loads are dominated by the hull unsteady aerodynamic ("apparent mass") contributions, the nose cone forces were not noticeably changed.

ORIGINAL PAGE IS
OF POOR QUALITY

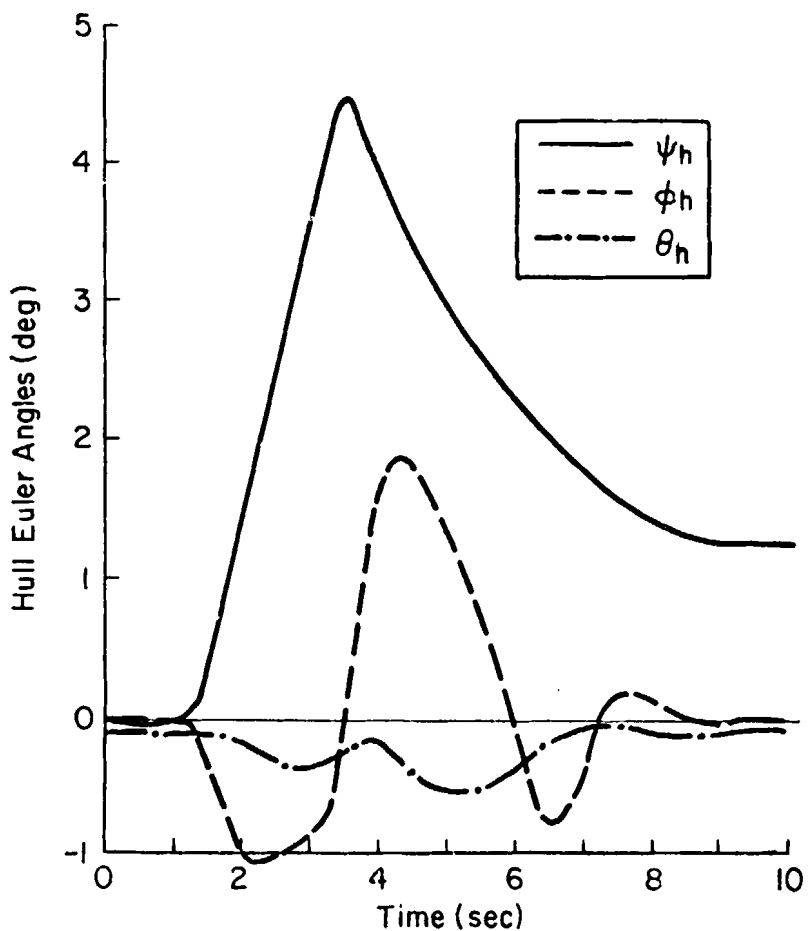
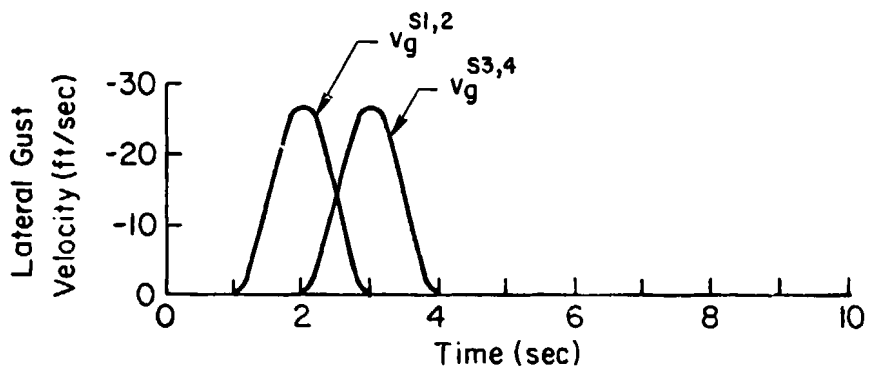


Figure 19. Nonlinear Response of Moored Vehicle to a Discrete Lateral Gust, $V_w = 60$ kts

ORIGINAL PAGE IS
OF POOR QUALITY

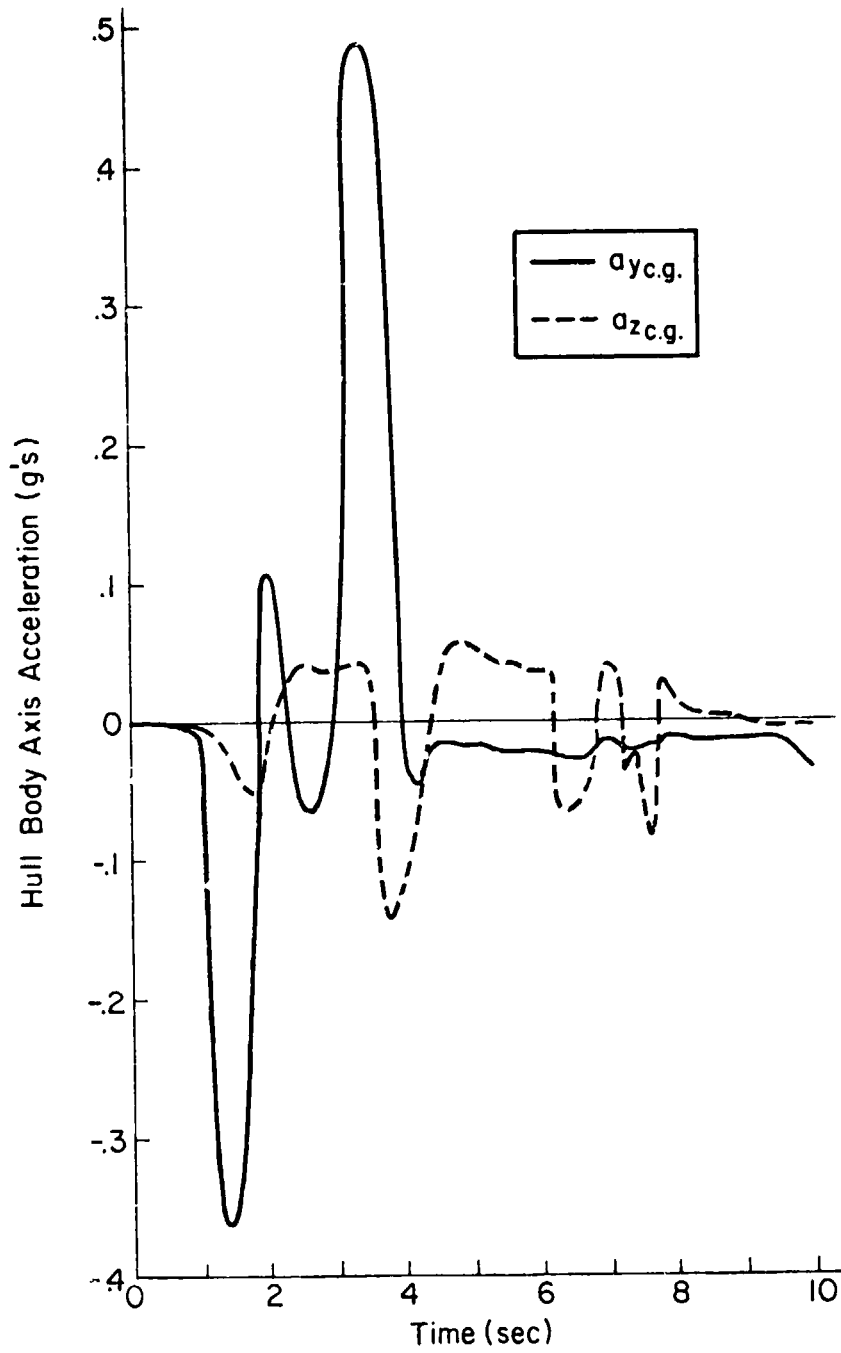


Figure 19. Continued

ORIGINAL PAGE IS
OF POOR QUALITY

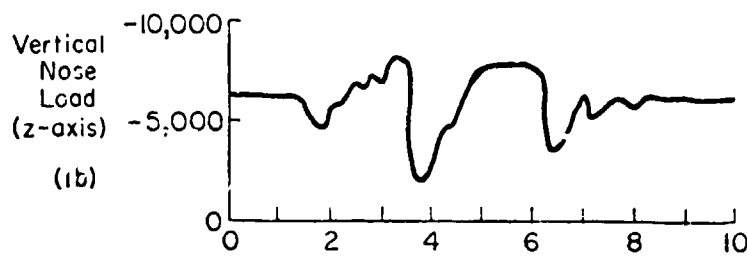
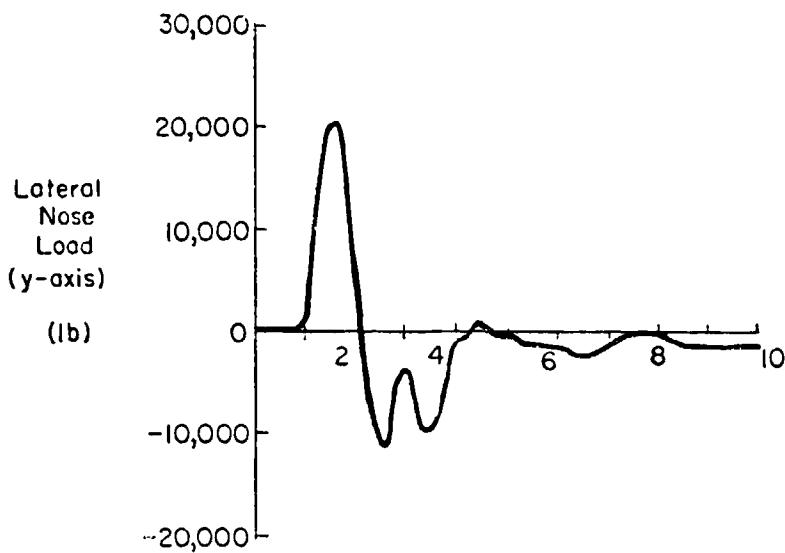
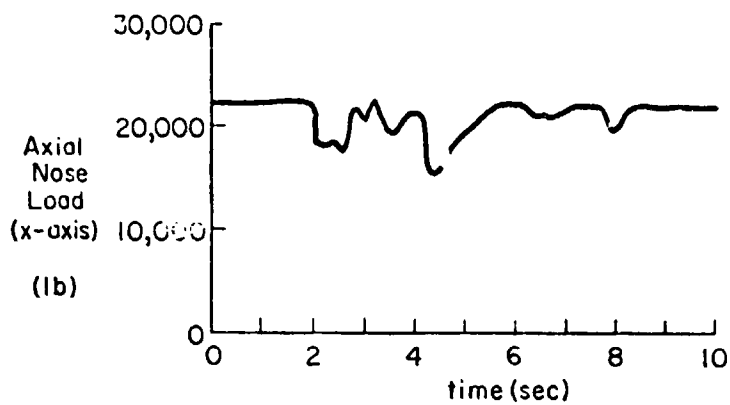


Figure 19. Concluded

SECTION IX

CONCLUSIONS

This dynamics and control analysis of the Helistat quadrotor heavy-lift airship suggests:

- 1) The cruise speed for the H34 rating of 1275 HP is 40-50 kts, depending on loading condition.
- 2) Maximum payload capability is 45,000 lbs for standard day sea level-based operations.
- 3) Crosswind capability in hover is 10 kts for the unloaded condition and 5-8 kts for the loaded condition. However, the roll-to-translate control gearing causes excessive roll angles at these crosswinds.
- 4) Sideslip angles of 110-135 degrees are critical for directional trim and stability, and should be avoided.
- 5) The small perturbation dynamics of the Helistat are very poorly damped, and may lead to handling qualities problems in high workload environments.
- 6) The dynamics of the Helistat are highly coupled with the sling-load, thus making precise load-positioning difficult.
- 7) The addition of two upper fins reduces the degradation of pitch and yaw stability with air-speed.
- 8) Mooring loads may be much higher than the design values; allowable operating conditions and/or mooring and ground handling equipment should be reconsidered to reflect these higher anticipated levels.

REFERENCES

- 1) Tischler, Mark B., Robert F. Ringland, Henry R. Jex, et al., Flight Dynamics Analysis and Simulation of Heavy Lift Airships, Volume II: Technical Manual, Systems Technology, Inc. Technical Report No. 1151-2, August 1982.
- 2) Ferry, Robert G. and James S. Hayden, Limited Phase IV Performance and Stability (H-34A), Air Force Flight Center TR46-15 (Addendum) and TR56-8 (Addendum), Sept. 1956.
- 3) A Preliminary Design Study of a Hybrid Airship for Flight Research, NASA CR 166246, July 1981.
- 4) Davis, J., T. Garnett, J. Gaul, Heavy Lift Helicopter Flight Control System. Vol. III: Automatic Flight Control System Development and Feasibility Demonstration, USAAMRDL-TR-77-40C, Sept. 1977.
- 5) Tischler, Mark B. and Roger H. Hoh, "Handling Qualities Criteria for Flight Path Control of V/STOL Aircraft," AIAA Paper No. 82-1292, presented at AIAA 9th Atmospheric Flight Mechanics Conf., Aug. 1982.
- 6) Fries, Gordon H. and John J. Schneider, "HLH and Beyond," SAE Paper No. 791086, at Aerospace Meeting Hyatt House, Los Angeles, Dec. 3-6, 1979.
- 7) McRuer, Duane, Irving Ashkenas, and Dunstan Graham, Aircraft Dynamics and Automatic Control, Princeton University Press, 1973.
- 8) Wolkovitch, Julian, Donald E. Johnston, Automatic Control Considerations for Helicopters and VTOL Aircraft with and Without Sling Loads, Systems Technology, Inc. Technical Report No. 138-1, Nov. 1965. Wezeman, Claude D., Richard A. Peeters, Walter A. Johnson, and Richard P. Walton, appendices, Nov. 1965.
- 9) Hoerner, Sighard F., and H. V. Borst, Fluid-Dynamic Lift, Hoerner Fluids Dynamics, 1975.
- 10) Schlichting, Hermann, and Erich Truckenbrodt, Aerodynamics of the Airplane, McGraw-Hill International Book Company, New York, 1979.
- 11) Soergl, D. G., and K. R. Meenen, Piasecki Aircraft Company Progress Report PIAC 97-X-200-14 for the Period 1 March to 1 April 1981.
- 12) Frost, Walter, and Robert E. Turner, "Summary of Atmospheric Wind Design Criteria for Wind Energy Conversion System Development," NASA Technical Paper 1389, Jan. 1979.
- 13) Soergl, D. G., and K. R. Meenen, Piasecki Aircraft Company Progress Report PIAC 97-X-200-12 for the Period 1 January to 1 February 1981.

APPENDIX A. HELISTAT SIMULATION INPUT DATA

The input data is partitioned according to groups of general vehicle characteristics as follows:

- A. Geometry
- B. Vehicle mass characteristics
- C. Vehicle aerodynamics
- D. Payload mass characteristics
- E. Payload aerodynamics

A. GEOMETRY

The major assumptions which were adopted in the development of the Helistat geometry data base are as follows:

1. The hull was modeled as an ellipsoid of revolution (i.e., circular cross section) with the following characteristics

Length	= 339.37 ft
Diameter	= 75.42 ft
Volume	= 975,000 ft ³

2. The tail configuration consists of two fins in a "V" configuration located on the lower side of the hull envelope.
3. The effective attachment points of the interconnecting structure (ICS) to the helicopters are located at the intersection of the central line of the ICS (nominal elastic axis) and the helicopter fuselage. This assumption allows the tabulation of internal loads between the structure and the helicopter and allows an evaluation of the applied loads at the tips of the interconnecting structure. When these results are taken along with the load to the hull center of volume, it will be possible to assess the shear and bending distributions along the span of the interconnecting structure. Based on this attach-point assumption, the mass and inertial characteristics of the interconnecting structure are then lumped into those of the hull in order to generate an effective hull with appropriate total mass and center of gravity (c.g.) characteristics.
4. The landing gear configuration consists of three oleo struts in parallel. The three oleos have total spring and damping constants of 12,000 lb/ft and 3000 lb-sec/ft, respectively. This yields a static deflection of 5.5 inches at the maximum heaviness mooring condition (buoyance ratio equal to 0.66), corresponding to 22 percent of the total oleo/tire travel.

B. Vehicle Mass Characteristics

The following four vehicle configurations are typical of those that may be expected during Helistat logging operations in the Pacific Northwest:

1. Standard operations at a pressure height (ceiling) of 1,000 ft above ground level (AGL) (6,000 ft total altitude)--ballonets are fully deflated; 50 percent of the maximum fuel supply; crew of five.
 - a. Vehicle only
 - b. Vehicle plus 30,000 lb (nominal) payload--this assumed payload weight is approximately 90 percent of the maximum payload capability in hover at 6,000 ft total altitude.

The standard operational configuration, with and without a payload, was selected to represent the Helistat operating in typical cruise and hover environments for logging conditions in the Pacific Northwest. The major thrust of the present analysis will be an evaluation of this configuration over a range of vehicle speeds and atmospheric conditions.

2. Minimum flying weight at ground level (5,000 ft total altitude)--ballonets set for operations to 1,000 AGL pressure height; 10 percent of maximum fuel capability; crew of five; no payload.

The minimum flying weight configuration was selected to be representative of vehicle landing operations. In this configuration the fuel level is minimum, resulting in a light vehicle with a relatively high vertical c.g. location. This configuration may be critical for vehicle-alone flying qualities.

3. Standard mooring weight at ground level (5,000 ft total altitude)--ballonets set for operation to 1,000 AGL pressure height; 10 percent of maximum fuel capability; no crew.

This represents a typical configuration for on-site mooring and will be used to study the problems of moored-vehicle motions and loads in response to discrete gust encounters.

4. Maximum heaviness configuration at ground level (5,000 total altitude)--ballonets set for operations to 9,000 ft AGL pressure height; maximum fuel capability; crew of five.

This is a typical ferry configuration for 14,000 ft total pressure height. This configuration represents the maximum anticipated landing weight and will therefore be used to analyze the landing gear oleos.

Summarizing, Configurations 1a and 1b will be analyzed for basic piloting performance and control characteristics. Configuration 2 will be used to investigate the importance of buoyancy ratio and vertical c.g. effects. Configurations 3 and 4 will be used for mooring and landing analyses.

The maximum fuel capability is assumed to be 310 gallons per helicopter which is typical of the H-34 equipped with full standard and auxiliary fuel tanks. The fuel tanks are assumed to be located on the helicopter center of gravity. Therefore small shifts in the helicopter c.g. characteristics due to fuel state changes among the flight conditions are ignored. Each helicopter is considered to hold 12.4 gallons of oil also located at the respective helicopter c.g.

The helicopter moments of inertia were obtained from data on the standard S-53 helicopter (Ref. 1). These basic inertias were not adjusted for modifications to the H-34's, because they represent very small percentages of the total vehicle's moments of inertia.

The moment of inertia characteristics of the interconnecting structure are estimated from a simple X-beam member model.

C. Vehicle Aerodynamics

1. The aerodynamics of the interconnecting structure were estimated from wind tunnel data of truss structures (e.g., electric transmission towers, radio towers, and suspension bridges) given in Ref. 2. These estimates require a knowledge of the effective solidity ratio of the structure (projected solid area divided by projected frontal areas). A conservative estimate of this ratio is 0.2, resulting in a drag coefficient based on the projected frontal area of 0.35. Using these values, the interconnecting structure has a total drag area (f_e) of 1,575 sq. ft. Reference 3 gives a drag area of 654 sq. ft. for the entire cruise configuration (hull, tail, helicopters, and ICS). This implies an ICS drag area significantly lower than the value cited herein. Based on the present estimate, the drag of the interconnecting structure accounts for 80 percent of the total vehicle drag in cruise and will therefore be particularly important for performance calculations. Perhaps some means of reducing the effective drag area in cruise (e.g., by aerodynamic fairings or other drag reduction means) should be considered to improve the performance of the operational configuration.
2. The reference center for hull aerodynamics is located at the hull center of volume, which is significantly above the aerodynamic center of the interconnecting structure. Since the drag of the interconnecting structure represents such a significant percentage of the total drag of the vehicle, the accurate modeling of its contributing moments is important for trim analyses. In order to accurately account for the location of the aerodynamic center of the ICS, the aerodynamic parameters of the helicopter fuselages were appropriately adjusted. The resulting effective vehicle has the same total drag coefficients along all three axes with an accurate description of the actual drag moments and the dynamic damping.

ORIGINAL PAGE IS
OF POOR QUALITY

3. Some variability exists in the literature on the accurate calculation of tail surface forces and control effectiveness. The methods given in Refs. 4 and 5 produce good correlation with the available wind tunnel data.
4. The aerodynamic interference effects were estimated from empirical curves given in the forthcoming technical manual for the HLA simulation (Ref. 6). These models are based heavily on wind tunnel data and analytical results published by Nielsen Engineering and Research. The similarity of the Helistat to the configurations from which the models were developed lends credibility to the estimated input data.

D. Payload Mass Characteristics

1. The payload configuration is assumed to consist of constant density, lumber with a specific weight of 54 lb/ft^3 (obtained from the Forestry Service). For an assumed nominal weight of 30,000 lb, this yields the following nominal payload configuration: four logs each with a length of 42 ft, diameter of 2.05 ft, volume of 138.8 ft^3 , mass of 231.1 slugs. The four logs are bound together in a square cross-section configuration with an end area of 16 sq ft and a length of 42 ft.
2. The choker cable is connected at a location of 20 percent of the length (8.4 ft aft of one end).
3. The effective spring constant of the payload cable damper is based on the shock absorber characteristics for standard cranes. For a standard crane payload weight of 50,000 lb, a suitable stiffness constant is $1 \times 10^5 \text{ lb-ft}$. The resulting natural frequency for the 30,000-lb HLA payload is about 10.4 rad/sec with an assumed damping ratio of about 0.7.

E. Payload Aerodynamics

The payload aerodynamics were calculated based on a streamline body of high fineness ratio (length/diameter = 10.5). The drag coefficients were obtained from Ref. 2 for a streamline body with considerable surface roughness. This simplified model is sufficiently accurate, since the forces associated with payload aerodynamics are very small in comparison with those associated with the payload inertial and cable characteristics.

F. Computer Listing of Input Data for Nominal Configuration
With 30,000 lb Slung-Payload

*****INPUT DATA*****

-----GEOMETRY INPUTS-----

BASIC HULL MEASUREMENTS
 HULARA = .201E+05 FT**2
 HULDT1 = .750E+02 FEET
 HULDT2 = 1
 HULDT3 = .330E+03 FEET
 HULDT4 = .0750E+04 FT**3

RASTIC TAIL MEASUREMENTS
 NUMT1 = 2
 RTALOC = .13350, 0.00, 0.00 FEET
 TALENA = .150E+04 FT**2
 TSPAN = .370E+02 FEET
 TALID = 1

RASTIC LPU VALUES
 NUMLPU = 4
 LPUID = 1

FOUR VECTORS FROM HULL CV REFERENCE AXES TO EACH LPU ATTACH POINT
 RATC1 = .310E+02, .0230E+02, .5000E+02 FEET
 RATC2 = .318E+02, .0230E+02, .5000E+02 FEET
 RATC3 = .240E+02, .0230E+02, .5000E+02 FEET
 RATC4 = .0266E+02, .0230E+02, .5000E+02 FEET

FOUR VECTORS FROM EACH LPU FUSELAGE REFERENCE AXES TO ITS HULL ATTACH POINT
 RLTC1 = .100E+01, .200E+01, .1470E+01 FEET
 RLTC2 = .1060E+01, .200E+01, .1670E+01 FEET
 RLTC3 = .1050E+01, .200E+01, .1470E+01 FEET
 RLTC4 = .1030E+01, .200E+01, .1070E+01 FEET

VECTORS TO THE POSITION OF EACH ROTOR HUB WITH RESPECT TO ITS LPU FUSELAGE REFERENCE AXES
 RROT1 = 0.
 RROT2 = 0.
 RROT3 = 0.
 RROT4 = 0.
 RROT5 = 0.

ROTOR CONFIGURATION
 NRBLD1 = 3
 NRBLD2 = 4
 NRBLD3 = 4
 NRBLD4 = 4

RADMT1 = 20.000 FEET
 RADMT2 = 20.000 FEET
 RADMT3 = 20.000 FEET
 RADMT4 = 20.000 FEET

CORDR1 = 1.5200 FEET
 CORDR2 = 1.5200 FEET
 CORDR3 = 1.5200 FEET
 CORDR4 = 1.5200 FEET

SIDE PROJECTED AREA
 MAXIMUM DIAMETER
 CONFIGURATION ID #
 LENGTH OF HULL
 TOTAL DISPLACEMENT VOLUME

NUMBER OF FINS
 TAIL VECTOR FROM HULL CV
 TAIL REFERENCE AREA
 TAIL SPAN
 TAIL CONFIGURATION ID #

NUMBER OF LPUS
 CONFIGURATION ID #

NUMBER OF BLADES ROTOR 1
 NUMBER OF BLADES ROTOR 2
 NUMBER OF BLADES ROTOR 3
 NUMBER OF BLADES ROTOR 4

EFFECTIVE RADIUS ROTOR 1
 EFFECTIVE RADIUS ROTOR 2
 EFFECTIVE RADIUS ROTOR 3
 EFFECTIVE RADIUS ROTOR 4

BLADE CHORD AT 3/4 RADIUS STATION ROTOR 1
 BLADE CHORD AT 3/4 RADIUS STATION ROTOR 2
 BLADE CHORD AT 3/4 RADIUS STATION ROTOR 3
 BLADE CHORD AT 3/4 RADIUS STATION ROTOR 4

-----VECTORS TO THE POSITION OF EACH PROPELLER HUB WITH RESPECT TO ITS LPU FUSELAGE REFERENCE AXES

RPRUP1 = .1625E+02 0.
 RPRUP2 = .1625E+02 0.
 RPRUP3 = .1625E+02 0.
 RPRUP4 = .1625E+02 0.

-----PROPELLER CONFIGURATION

NPBLD1 = 3
 NPBLD2 = 3
 NPBLD3 = 3
 NPBLD4 = 3
 RADP1 = 6.5000 FEET
 RADP2 = 6.5000 FEET
 RADP3 = 6.5000 FEET
 RADP4 = 6.5000 FEET
 CORUP1 = .0930 FEET
 CORUP2 = .0930 FEET
 CORUP3 = .0930 FEET
 CORUP4 = .0930 FEET

NUMBER OF BLADES PROPELLER 1
 NUMBER OF BLADES PROPELLER 2
 NUMBER OF BLADES PROPELLER 3
 NUMBER OF BLADES PROPELLER 4
 EFFECTIVE RADIUS PROPELLER 1
 EFFECTIVE RADIUS PROPELLER 2
 EFFECTIVE RADIUS PROPELLER 3
 EFFECTIVE RADIUS PROPELLER 4
 BLADE CHORD AT 3/4 RADIUS STATION PROPELLER 1
 BLADE CHORD AT 3/4 RADIUS STATION PROPELLER 2
 BLADE CHORD AT 3/4 RADIUS STATION PROPELLER 3
 BLADE CHORD AT 3/4 RADIUS STATION PROPELLER 4

-----WATERLINE CONTROL AXIS DEFLECTION FROM

A1SP1 = 0.0000 RADIANS
 A1SP2 = 0.0000 RADIANS
 A1SP3 = 0.0000 RADIANS
 A1SP4 = 0.0000 RADIANS

PROPELLER-1
 PROPELLER-2
 PROPELLER-3
 PROPELLER-4

-----ORIGINAL CONTROL AXIS DEFLECTION FROM

B1SP1 = 1.4490 RADIANS
 B1SP2 = 1.4490 RADIANS
 B1SP3 = 1.4490 RADIANS
 B1SP4 = 1.4490 RADIANS

PROPELLER-1
 PROPELLER-2
 PROPELLER-3
 PROPELLER-4

-----FUSELAGE ANGLES WITH RESPECT TO THE HULL CENTER OF VOLUME REFERENCE AXES

GBANG1 = 0.
 GBANG2 = 0.
 GBANG3 = 0.
 GBANG4 = 0.

0.
 0.
 0.
 0.
 RADIANS
 RADIANS
 RADIANS
 RADIANS

.....PAYLOAD GEOMETRY INPUTS.....

-----BASIC PAYLOAD MEASUREMENTS

PAYLTH = 42.0000 FEET
 PAYLDM = 4.0000 FEET
 PAYLDB = 45.2000 FT.***5
 PAYLAD = 16.0000 FT.***2
 PAYLID = 2

PAYLOAD LENGTH
 PAYLOAD DEPTH
 PAYLOAD DISPLACED VOLUME
 PAYLOAD FRONT PROJECTED AREA
 PAYLOAD CONFIGURATION ID #

-----FOUR ATTACH POINTS ON THE PAYLOAD WITH RESPECT TO THE PAYLOAD REFERENCE CENTER

RPTCH1 = 0.00 0.00 -12.60 FEET
 RPTCH2 = -2.00 0.00 -12.60 FEET
 RPTCH3 = 2.00 0.00 -12.60 FEET
 RPTCH4 = -1.00 0.00 -12.60 FEET

-----FOUR ATTACH POINTS ON THE HULL WITH RESPECT TO THE HULL CENTER OF VOLUME

RATHP1 = 3.00 0.00 50.11 FEET
 RATHP2 = 3.50 0.00 50.11 FEET
 RATHP3 = 3.00 0.00 50.11 FEET
 RATHP4 = 3.00 0.00 50.11 FEET

-----PAYLOAD CABLE LENGTHS

USLTH1 = 250.0000 FEET
 USLTH2 = 250.0000 FEET
 USLTH3 = 250.0000 FEET
 USLTH4 = 250.0000 FEET

CABLE 1
 CABLE 2
 CABLE 3
 CABLE 4

ORIGINAL PAGE IS
OF POOR QUALITY

-----MOORING POINT GEOMETRY-----

-----MOORING POINT ON MAST IN INERTIAL COORDINATES
MASTLX = 0.0
MASTLY = -7.740E+02 FEET
-----MOORING POINT ON HULL RELATIVE TO THE HULL CENTER OF VOLUME
RMORPT = .1630E+03 0.0

-----LANDING GEAR ATTACH POINTS AND SPRING CONSTANTS-----

-----LANDING GEAR ATTACH POINTS ON THE HULL
RATNG1 = .2110E+02 .3986E+02 .7199E+02 FEET
RATNG2 = .2110E+02 .3986E+02 .7199E+02 FEET
RATNG3 = .1720E+02 .3986E+02 .7199E+02 FEET
RATNG4 = .1720E+02 .3986E+02 .7199E+02 FEET
-----LANDING GEAR LENGTHS
LGRL1 = .2043E+01 FEET
LGRL2 = .2043E+01 FEET
LGRL3 = .2043E+01 FEET
LGRL4 = .2043E+01 FEET
-----LANDING GEAR SPRING CONSTANTS
GEAR1 = .1206E+05 LB / FT
GEAR2 = .1206E+05 LB / FT
GEAR3 = .1206E+05 LB / FT
GEAR4 = .1206E+05 LB / FT
-----LANDING GEAR RIDE STIFFNESS CONSTANTS
GFRM1 = .1054E+06 LB / FT
GFRM2 = .1054E+06 LB / FT
GFRM3 = .1054E+06 LB / FT
GFRM4 = .1054E+06 LB / FT
-----LANDING GEAR SPRING DAMPING CONSTANTS
GEARC1 = .3000E+04 (LB * SEC) / FT
GEARC2 = .3000E+04 (LB * SEC) / FT
GEARC3 = .3000E+04 (LB * SEC) / FT
GEARC4 = .3000E+04 (LB * SEC) / FT
-----LANDING GEAR FRACTURE CONSTANTS
MUKG1 = .1000E+00
MUKG2 = .1000E+00
MUKG3 = .1000E+00
MUKG4 = .1000E+00

LANDING GEAR 1
LANDING GEAR 2
LANDING GEAR 3
LANDING GEAR 4



ORIGINAL PAGE IS
OF POOR QUALITY

-----PAYLOAD MASS AND MOMENT OF INERTIA INPUTS-----
 -----PAYLOAD CENTER OF GRAVITY VECTOR WITH RESPECT TO THE PAYLOAD REFERENCE CENTER
 RPAYCE = 0.0000 0.0000 0.0000 FEET
 -----MASS AND MOMENT OF INERTIA OF THE PAYLOAD
 MSPAY = .9320E+03 SLUGS
 IPAYX = .1300E+00 SLUGS
 IPAYY = .1300E+00 SLUGS
 IPAYZ = .2417E+04 SLUGS
 IPAYX = 0. SLUGS

-----PAYLOAD CABLE INPUTS-----
 -----CABLE SPRING CONSTANTS
 CABLK1 = .5000E+05 (SFCAS2) / (FTAS2)
 CABLK2 = .5000E+05 (SFCAS2) / (FTAS2)
 CABLK3 = 0. (SFCAS2) / (FTAS2)
 CABLK4 = 0. (SFCAS2) / (FTAS2)
 -----CABLE DAMPING CONSTANTS
 CABLD1 = .0050E+04 (SFLAS2) / (FTAS2)
 CABLD2 = .0050E+04 (SFLAS2) / (FTAS2)
 CABLD3 = 0. (SFLAS2) / (FTAS2)
 CABLD4 = 0. (SFLAS2) / (FTAS2)

CABLE 1
 CABLE 2
 CABLE 3
 CABLE 4
 CABLE 1
 CABLE 2
 CABLE 3
 CABLE 4



ORIGINAL PAGE IS
OF POOR QUALITY

-----MASS AND MOMENT OF INERTIA INPUTS-----
 -----HULL CENTER OF GRAVITY VECTOR WITH RESPECT TO HULL CENTER OF VOLUME REFERENCE AXES
 RMULCR = .4200E+01 0. 1442E+02 FEET

-----MASS AND MOMENT OF INERTIA OF HULL
 MASHUJ = .1372E+04 SLUGS
 IMLUXY = .1620E+07 SLUG*(FT.**2)
 IMLUYX = .1052E+08 SLUG*(FT.**2)
 IMLUZZ = .9130E+07 SLUG*(FT.**2)
 IMLUZZ = 0. SLUG*(FT.**2)

COMPLETE MASS OF HULL STRUCTURE
 MOMENT OF INERTIA ABOUT CG X AXES
 MOMENT OF INERTIA ABOUT CG Y AXES
 MOMENT OF INERTIA ABOUT CG Z AXES
 PRODUCT OF INERTIA WRT THE CG XZ AXES

-----FOUR VECTORS LOCATING EACH LPU'S CG WITH RESPECT TO ITS FUSELAGE REFERENCE AXES
 RCGLP1 = .4130E+00 0. -.5520E+01 FEET
 RCGLP2 = .4130E+00 0. -.5520E+01 FEET
 RCGLP3 = .4000E+00 0. -.3910E+01 FEET
 RCGLP4 = .4130E+00 0. -.5520E+01 FEET

-----MASS AND MOMENT OF INERTIA OF LPU=1
 MASLP1 = .2471E+03 SLUGS
 ILP1XX = .5875E+05 SLUG*(FT.**2)
 ILP1YY = .2750E+05 SLUG*(FT.**2)
 ILP1ZZ = .2750E+05 SLUG*(FT.**2)
 ILP1XY = 0. SLUG*(FT.**2)

MASS OF LPU=1
 MOMENT OF INERTIA ABOUT CG X AXES
 MOMENT OF INERTIA ABOUT CG Y AXES
 MOMENT OF INERTIA ABOUT CG Z AXES
 PRODUCT OF INERTIA WRT THE CG XZ AXES

-----MASS AND MOMENT OF INERTIA OF LPU=2
 MASLP2 = .2471E+03 SLUGS
 ILP2XX = .5875E+05 SLUG*(FT.**2)
 ILP2YY = .2750E+05 SLUG*(FT.**2)
 ILP2ZZ = .2750E+05 SLUG*(FT.**2)
 ILP2XY = 0. SLUG*(FT.**2)

MASS OF LPU=2
 MOMENT OF INERTIA ABOUT CG X AXES
 MOMENT OF INERTIA ABOUT CG Y AXES
 MOMENT OF INERTIA ABOUT CG Z AXES
 PRODUCT OF INERTIA WRT THE CG XZ AXES

-----MASS AND MOMENT OF INERTIA OF LPU=3
 MASLP3 = .2471E+03 SLUGS
 ILP3XX = .5875E+05 SLUG*(FT.**2)
 ILP3YY = .2750E+05 SLUG*(FT.**2)
 ILP3ZZ = .2750E+05 SLUG*(FT.**2)
 ILP3XY = 0. SLUG*(FT.**2)

MASS OF LPU=3
 MOMENT OF INERTIA ABOUT CG X AXES
 MOMENT OF INERTIA ABOUT CG Y AXES
 MOMENT OF INERTIA ABOUT CG Z AXES
 PRODUCT OF INERTIA WRT THE CG XZ AXES

-----MASS AND MOMENT OF INERTIA OF LPU=4
 MASLP4 = .2471E+03 SLUGS
 ILP4XX = .5875E+05 SLUG*(FT.**2)
 ILP4YY = .2750E+05 SLUG*(FT.**2)
 ILP4ZZ = .2750E+05 SLUG*(FT.**2)
 ILP4XY = 0. SLUG*(FT.**2)

MASS OF LPU=4
 MOMENT OF INERTIA ABOUT CG X AXES
 MOMENT OF INERTIA ABOUT CG Y AXES
 MOMENT OF INERTIA ABOUT CG Z AXES
 PRODUCT OF INERTIA WRT THE CG XZ AXES

-----MOTOR LOCK NUMBER
 LOCKM1 = 10.4000
 LOCKM2 = 10.9000
 LOCKM3 = 14.4000
 LOCKM4 = 10.9000

MOTOR 1
 MOTOR 2
 MOTOR 3
 MOTOR 4

ORIGINAL PAGE IS
OF POOR QUALITY

.....EXHAUST THRUST INPUTS.....

EXHAUST JET FORCES
JETHS1 = 0. LHS.
JETHS2 = 0. LHS.
JETHS3 = 0. LHS.
JETHS4 = 0. LHS.
JETHS5 = 0. LHS.

LPU 1
LPU 2
LPU 3
LPU 4

.....POSITION OF THE EXHAUST NOZZLES WITH RESPECT TO THE FUSELAGE REFERENCE CENTERS

REXLC1 = 0. FEET
REXLC2 = 0. FEET
REXLC3 = 0. FEET
REXLC4 = 0. FEET

LPU 1
LPU 2
LPU 3
LPU 4

.....ANGULAR ORIENTATIONS OF THE EXHAUST NOZZLES WITH RESPECT TO THE FUSELAGE REFERENCE CENTERS

AISE1 = 0. RADIAN
AISE2 = 0. RADIAN
AISE3 = 0. RADIAN
AISE4 = 0. RADIAN
AISE5 = 0. RADIAN

LPU 1
LPU 2
LPU 3
LPU 4

ORIGINAL PAGE IS
OF POOR QUALITY

.....PAYLOAD AERODYNAMIC PARAMETERS INPUT.....

.....PAYLOAD X, Y AND Z MOMENT DERIVATIVES WITH RESPECT TO:
XUABP = .2750E+00 LB*(SAA2)/(FT**2) U * ABS(U)
YVABP = .2050E+00 LB*(SAA2)/(FT**2) V * ABS(V)
ZHWABP = .1600E-01 LB*(SAA2)/(FT**2) W * ABS(W)
.....PAYLOAD YAWING MOMENT DERIVATIVE WITH RESPECT TO:
NIYP = 0 LB*(SAA2)/FT U * V
LPPAMP = .4 (-.903 FT*LB*(SAA2)/(RAD**2) P * ABS(P)
PCPAMP = .4 2.03 FT*LB*(SAA2)/(RAD**2) Q * ABS(Q)
NRPAMP = 0. FT*LB*(SAA2)/(RAD**2) R * ABS(R)

ORIGINAL PAGE IS
OF POOR QUALITY

.....LPU AERODYNAMIC PARAMETERS INPUT.....

FOUR VECTORS LOCATING FUSELAGE AERODYNAMIC CENTER WITH RESPECT TO LPU FUSELAGE REFERENCE AXES

RACLP1 = .1420E+01 U.
 RACLP2 = .1420E+01 U.
 RACLP3 = .1420E+01 U.
 RACLP4 = .1420E+01 U.

ROTOR BLADE LIFT CURVE SLOPE AND DRAG COEFFICIENTS

ROTOR 1

LCR01 = 5.0500 1/RAD.
 DLTR01A = .0007 1/RAD.
 DLTR01B = .0216 1/RAD.
 DLTR01C = .0000 1/RAD.

ROTOR 2

LCR02 = 5.0500 1/RAD.
 DLTR02A = .0007 1/RAD.
 DLTR02B = .0216 1/RAD.
 DLTR02C = .0000 1/RAD.

ROTOR 3

LCR03 = 5.0500 1/RAD.
 DLTR03A = .0007 1/RAD.
 DLTR03B = .0216 1/RAD.
 DLTR03C = .0000 1/RAD.

ROTOR 4

LCR04 = 5.0500 1/RAD.
 DLTR04A = .0007 1/RAD.
 DLTR04B = .0216 1/RAD.
 DLTR04C = .0000 1/RAD.

PROPELLER BLADE LIFT CURVE SLOPE AND DRAG COEFFICIENTS

PROPELLER 1

LCR01 = 5.0500 1/RAD.
 DLTR01A = .0007 1/RAD.
 DLTR01B = .0216 1/RAD.
 DLTR01C = .0000 1/RAD.

PROPELLER 2

LCR02 = 5.0500 1/RAD.
 DLTR02A = .0007 1/RAD.
 DLTR02B = .0216 1/RAD.
 DLTR02C = .0000 1/RAD.

PROPELLER 3

LCR03 = 5.0500 1/RAD.
 DLTR03A = .0007 1/RAD.
 DLTR03B = .0216 1/RAD.
 DLTR03C = .0000 1/RAD.

PROPELLER 4

LCR04 = 5.0500 1/RAD.
 DLTR04A = .0007 1/RAD.
 DLTR04B = .0216 1/RAD.
 DLTR04C = .0000 1/RAD.

ORIGINAL PAGE IS
OF POOR QUALITY

DERIVATIVES WITH RESPECT TO U * ABS(U)

UUAF 1 0
UUAF 2 0
UUAF 3 0
UUAF 4 0

DERIVATIVES WITH RESPECT TO V * ABS(V)

VVAF 1 0
VVAF 2 0
VVAF 3 0
VVAF 4 0

DERIVATIVES WITH RESPECT TO W * ABS(W)

WWAF 1 0
WWAF 2 0
WWAF 3 0
WWAF 4 0

.....HULL AERODYNAMIC PARAMETERS INPUT.....

.....HULL ACCELERATION DERIVATIVES
 XUDOTM = -.1623E+03 LMA(SAA2)/FT
 YVDOTM = -.1745E+04 LMA(SAA2)/FI
 ZWDOTM = -.1785E+06 LMA(SAA2)/FT
 LWDOTM = 0.
 MDDOTM = -.7900E+07 FIALPA(SAA2)/RAD
 NMDOTM = -.7900E+07 FIALPA(SAA2)/RAD

.....TAIL ACCELERATION DERIVATIVES
 YVDOTY = -.2268E+02 LMA(SAA2)/FI
 ZVDOTY = -.2277E+03 LMA(SAA2)/FI
 LVDOTY = -.0531E+03 LMA(SAA2)
 LPDOUTY = -.4100E+05 FIALA(SAA2)/RAD
 MDDOUTY = -.1450E+05 FIALMA(SAA2)/RAD
 NMDOUTY = -.1450E+05 FIALMA(SAA2)/RAD

.....HULL X FORCE DERIVATIVES WITH RESPECT TO:
 XUDARM = -.2030E+06 LMA(SAA2)/(FTAA2)
 XVDAM = -.1785E+04 LMA(SAA2)/(RADAA2)
 XWVAM = -.1785E+04 LMA(SAA2)/(FTAA2)

.....HULL Y FORCE DERIVATIVES WITH RESPECT TO:
 YVDARM = -.3300E+02 LMA(SAA2)/(FTAA2)
 YVDRAM = 0.
 YVDRAM = 0.
 YVDRAM = 0.
 YVDRAM = 0.
 YVDRAM = 0.

.....HULL Z FORCE DERIVATIVES WITH RESPECT TO:
 ZWDARM = -.2520E+02 LMA(SAA2)/(FTAA2)
 ZVDARM = 0.
 ZVDARM = 0.
 ZVDARM = 0.
 ZVDARM = 0.
 ZVDARM = 0.

.....HULL ROLLING MOMENT DERIVATIVES WITH RESPECT TO:
 LPPARM = -.2270E+05 FIALPA(SAA2)/(RADAA2)
 LPPARM = 0.
 LPPARM = 0.
 LPPARM = 0.
 LPPARM = 0.
 LPPARM = 0.

.....HULL PITCHING MOMENT DERIVATIVE WITH RESPECT TO:
 MDDARM = -.1983E+08 FIALMA(SAA2)/(RADAA2)
 MDDARM = -.1558E+04 LMA(SAA2)/FT
 MDDARM = 0.
 MDDARM = 0.
 MDDARM = 0.
 MDDARM = 0.

.....HULL YAWING MOMENT DERIVATIVE WITH RESPECT TO:
 NMDARM = -.1983E+08 FIALMA(SAA2)/(RADAA2)
 NMDARM = -.1558E+04 LMA(SAA2)/FT
 NMDARM = 0.
 NMDARM = 0.
 NMDARM = 0.
 NMDARM = 0.

ORIGINAL PAGE IS
 OF POOR QUALITY

```

-----TAIL X FORCE DERIVATIVES WITH RESPECT TO1
XUUA6Y = -.1570E+01 LXA(SA+2)/(F1+2)          U * ABS(U)
-----TAIL Y FORCE DERIVATIVES WITH RESPECT TO1
YVVA6Y = -.1420E+01 LYA(SA+2)/(F1+2)          V * ABS(V)
YVPA6Y = -.2550E+03 LXA(SA+2)/(RAD+2)        P * ABS(P)
YAPV6Y = -.5330E+00 LXA(SA+2)/(RAD+2)        ALPHA*V * (VPT**2)
YEVSOY = -.1550E+01 LXA(SA+2)/(RAD+2)        BETA * (VXY**2)
YBVS6Y = -.1720E+00 LXA(SA+2)/(RAD+2)*(F1+2) BETA*ABS(BETA)*(VXY**2)
YAPSVY = -.1340E+00 LXA(SA+2)/(RAD+2)*(F1+2) ALPHA*P*ABS(ALPHA*P)*(VPT**2)

-----TAIL Z FORCE DERIVATIVES WITH RESPECT TO1
ZUUA6Y = -.2330E+01 LXA(SA+2)/(F1+2)          W * ABS(W)
ZVVA6Y = -.2540E+01 LYA(SA+2)/(RAD+2)        ALPHA * VZ**2
ZASVS1 = -.1717E+01 LXA(SA+2)/(RAD+2)*(F1+2) ALPHA*ABS(ALPHA)*(VZ**2)

-----TAIL ROLL RATE DERIVATIVES WITH RESPECT TO1
LVVABY = .1070E+02 LXA(SA+2)/FT              V * ABS(V)
LPPABY = -.4017E+00 LXA(SA+2)/(RAD+2)        P * ABS(P)
LAPVBY = -.2024E+02 LXA(SA+2)/(RAD+2)        ALPHA*P * VPT**2
LUVSOY = .1180E+02 LXA(SA+2)/(RAD+2)        BETA * VXY**2
LHABVY = .1170E+01 LXA(SA+2)/(RAD+2)*(F1)   BETA*ALPHA*(VXY**2)
LAPSVY = -.4000E+01 LXA(SA+2)/(RAD+2)*(F1) ALPHA*P*ABS(ALPHA*P)*(VPT**2)

-----TAIL LIFT COEFFICIENT SCALE FACTORS
LAL1XN = .9000
LAL2XN = .9000
LAL3XN = 1.0000

-----TAIL PARAMETRIC RADIANS
AL1T = .0200E+00 RADIANS
AL2T = .0300E+00 RADIANS
BETA1T = .0200E+00 RADIANS
BETA2T = .0300E+00 RADIANS
ALP1T = .0200E+00 RADIANS
ALP2T = .0300E+00 RADIANS

-----TAIL SURFACE EFFECTIVENESS PARAMETERS
TAUA = .1000E+00 (SCC+2) / (F1+2)
TAUB = .1000E+00 (SCC+2) / (F1+2)
TAUC = .1000E+00 (SCC+2) / (F1+2)

X-AXIS CORRECTION FOR PITCHING MOMENTS
Y-AXIS CORRECTION FOR PITCHING MOMENTS
Z-AXIS CORRECTION FOR PITCHING MOMENTS

LONGITUDINAL TAIL STALLING PARAMETERS
LATERAL TAIL STALL PARAMETERS
TAIL ROLLING STALL PARAMETERS

ATTENTION
ELEVATION
MUDDER

```

ORIGINAL PAGE IS
OF POOR QUALITY

-----INTERFERENCE CONSTANTS ON ROTOR-----

-----SHAFER CONSTANTS ROTOR 1

SKR1R1 = .3200E+01 RADIANS
SKR2R1 = .3000E+01 RADIANS
SKR3R1 = .3200E+00
LKR1R1 = .1500E+01 RADIANS
LKR2R1 = .2500E+01 RADIANS
LKRDR1 = .3200E+00

-----SHAFER CONSTANTS ROTOR 2

SKR1R2 = .3000E+01 RADIANS
SKR2R2 = .4000E+01 RADIANS
SKR3R2 = .3200E+00
LKR1R2 = .1500E+01 RADIANS
LKR2R2 = .2500E+01 RADIANS
LKRDR2 = .3200E+00

-----SHAFER CONSTANTS ROTOR 3

SKR1R3 = .4800E+00 RADIANS
SKR2R3 = .1570E+01 RADIANS
SKR3R3 = .3200E+00
LKR1R3 = .1500E+01 RADIANS
LKR2R3 = .2500E+01 RADIANS
LKRDR3 = .3200E+00

-----SHAFER CONSTANTS ROTOR 4

SKR1R4 = .7100E+01 RADIANS
SKR2R4 = .5410E+01 RADIANS
SKR3R4 = .3200E+00
LKR1R4 = .1500E+01 RADIANS
LKR2R4 = .2500E+01 RADIANS
LKRDR4 = .3200E+00

-----MILL ON ROTOR CONSTANTS

KR1A1 = .1200E+02 LH / (F1+2)
KR1B1 = .4600E+01
KR1A2 = .1200E+02 LH / (F1+2)
KR1B2 = .4600E+01
KR1A3 = .1200E+02 LH / (F1+2)
KR1B3 = .4600E+01
KR1A4 = .1200E+02 LH / (F1+2)
KR1B4 = .4600E+01

-----CONSTANTS ON ROTOR

KCR1 = .2000E+01
KCR2 = .2000E+01
KCR3 = .2000E+01
KCR4 = .2000E+01

BETA MAKE ANGLE 1
BETA MAKE ANGLE 2
BETA MAKE MAXIMUM DEFECT
LAMBDA MAKE ANGLE 1
LAMBDA MAKE ANGLE 2
LAMBDA MAKE MAXIMUM DEFECT

BETA MAKE ANGLE 1
BETA MAKE ANGLE 2
BETA MAKE MAXIMUM DEFECT
LAMBDA MAKE ANGLE 1
LAMBDA MAKE ANGLE 2
LAMBDA MAKE MAXIMUM DEFECT

BETA MAKE ANGLE 1
BETA MAKE ANGLE 2
BETA MAKE MAXIMUM DEFECT
LAMBDA MAKE ANGLE 1
LAMBDA MAKE ANGLE 2
LAMBDA MAKE MAXIMUM DEFECT

BETA MAKE ANGLE 1
BETA MAKE ANGLE 2
BETA MAKE MAXIMUM DEFECT
LAMBDA MAKE ANGLE 1
LAMBDA MAKE ANGLE 2
LAMBDA MAKE MAXIMUM DEFECT

ROTOR 1 A
ROTOR 1 H
ROTOR 2 A
ROTOR 2 B
ROTOR 3 A
ROTOR 3 B
ROTOR 4 A
ROTOR 4 B

INTERFERENCE CONSTANTS ON PROPELLER

CHARM CONSTANT PROPPELLER 1

BK1P1 = .2320E+01 RADIANS
 BK2P1 = .1320E+01 RADIANS
 MKHP1 = .1200E+00
 LK1P1 = .1800E+01 RADIANS
 LK2P1 = .2520E+01 RADIANS
 XL1DP1 = .1200E+00

SHADU CONSTANT PROPPELLER 2

BK1P2 = .1200E+01 RADIANS
 BK2P2 = .0800E+01 RADIANS
 MKHP2 = .1200E+00
 LK1P2 = .1200E+01 RADIANS
 LK2P2 = .0300E+01 RADIANS
 XL1DP2 = .1200E+00

QUAGU CONSTANT PROPPELLER 3

BK1P3 = .1800E+00 RADIANS
 BK2P3 = .1570E+01 RADIANS
 MKHP3 = .1200E+00
 LK1P3 = .1200E+01 RADIANS
 LK2P3 = .2520E+01 RADIANS
 XL1DP3 = .1200E+00

EMENGM CONSTANT PROPPELLER 4

BK1P4 = .0700E+01 RADIANS
 BK2P4 = .0400E+01 RADIANS
 MKHP4 = .1200E+00
 LK1P4 = .1200E+01 RADIANS
 LK2P4 = .0300E+01 RADIANS
 XL1DP4 = .1200E+00

SHILL ON PROPPELLER CONSTANTS

KHPA1 = .1200E+02 LB / (FT*2)
 KHPA2 = .2000E+01
 KHPB2 = .1200E+02 LB / (FT*2)
 KHPB2 = .0600E+01
 KHPA3 = .1200E+02 LB / (FT*2)
 KHPA3 = .0600E+01
 KHPA4 = .1200E+02 LB / (FT*2)
 KHPA4 = .0600E+01

RRGTP ON PROPPELLER CONSTANTS

KRP1 = .1600E+01
 KRP2 = .1600E+01
 KRP3 = .1600E+01
 KRP4 = .1600E+01

CGMNG ON PROPPELLER CONSTANTS

KGPI = .2000E+01
 KCP2 = .2000E+01
 KCP3 = .2000E+01
 KCP4 = .2000E+01

BETA WAKE ANGLE 1
 BETA WAKE ANGLE 2
 BETA WAKE MAXIMUM DEFECT
 LAMBDA WAKE ANGLE 1
 LAMBDA WAKE ANGLE 2
 LAMBDA WAKE MAXIMUM DEFECT

BETA WAKE ANGLE 1
 BETA WAKE ANGLE 2
 BETA WAKE MAXIMUM DEFECT
 LAMBDA WAKE ANGLE 1
 LAMBDA WAKE ANGLE 2
 LAMBDA WAKE MAXIMUM DEFECT

BETA WAKE ANGLE 1
 BETA WAKE ANGLE 2
 BETA WAKE MAXIMUM DEFECT
 LAMBDA WAKE ANGLE 1
 LAMBDA WAKE ANGLE 2
 LAMBDA WAKE MAXIMUM DEFECT

BETA WAKE ANGLE 1
 BETA WAKE ANGLE 2
 BETA WAKE MAXIMUM DEFECT
 LAMBDA WAKE ANGLE 1
 LAMBDA WAKE ANGLE 2
 LAMBDA WAKE MAXIMUM DEFECT

PROPPELLER 1 A
 PROPPELLER 1 R
 PROPPELLER 2 A
 PROPPELLER 2 D
 PROPPELLER 3 A
 PROPPELLER 3 H
 PROPPELLER 4 A
 PROPPELLER 4 H

LPU 1
 LPU 2
 LPU 3
 LPU 4

LPU 1
 LPU 2
 LPU 3
 LPU 4

ORIGINAL PAGE 19
 OF POOR QUALITY

ORIGINAL PAGE IS
OF POOR QUALITY

-----INTERFERENCE CONSTANTS ON FUSELAGE-----

-----MACHON CONSTANTS FUSELAGE 1
 BK1F1 = .2320E+01 RADIANS
 BK2F1 = .1220E+01 RADIANS
 BK3F1 = .1220E+01 RADIANS
 LK1F1 = .1890E+01 RADIANS
 LK2F1 = .2520E+01 RADIANS
 LK3F1 = .3220E+01 RADIANS

-----MACHON CONSTANTS FUSELAGE 2
 BK1F2 = .900E+01 RADIANS
 BK2F2 = .400E+01 RADIANS
 BK3F2 = .3200E+00
 LK1F2 = .300E+01 RADIANS
 LK2F2 = .430E+01 RADIANS
 LK3F2 = .3210E+00

-----MACHON CONSTANTS FUSELAGE 3
 BK1F3 = .4600E+00 RADIANS
 BK2F3 = .1570E+01 RADIANS
 BK3F3 = .3200E+00
 LK1F3 = .1830E+01 RADIANS
 LK2F3 = .2520E+01 RADIANS
 LK3F3 = .3200E+00

-----MACHON CONSTANTS FUSELAGE 4
 BK1F4 = .4710E+01 RADIANS
 BK2F4 = .5410E+01 RADIANS
 BK3F4 = .3200E+00
 LK1F4 = .3090E+01 RADIANS
 LK2F4 = .4390E+01 RADIANS
 LK3F4 = .3200E+00

-----MACHON CONSTANTS FUSELAGE 5
 BK1F5 = 0.
 BK2F5 = 0.
 BK3F5 = 0.
 BK4F5 = 0.

-----MACHON CONSTANTS FUSELAGE 6
 KPF1 = 0.
 KPF2 = 0.
 KPF3 = 0.
 KPF4 = 0.

BETA WAKE ANGLE 1
 BETA WAKE ANGLE 2
 BETA WAKE MAXIMUM DEFECT
 LAMBDA WAKE ANGLE 1
 LAMBDA WAKE ANGLE 2
 LAMBDA WAKE MAXIMUM DEFECT

BETA WAKE ANGLE 1
 BETA WAKE ANGLE 2
 BETA WAKE MAXIMUM DEFECT
 LAMBDA WAKE ANGLE 1
 LAMBDA WAKE ANGLE 2
 LAMBDA WAKE MAXIMUM DEFECT

BETA WAKE ANGLE 1
 BETA WAKE ANGLE 2
 BETA WAKE MAXIMUM DEFECT
 LAMBDA WAKE ANGLE 1
 LAMBDA WAKE ANGLE 2
 LAMBDA WAKE MAXIMUM DEFECT

BETA WAKE ANGLE 1
 BETA WAKE ANGLE 2
 BETA WAKE MAXIMUM DEFECT
 LAMBDA WAKE ANGLE 1
 LAMBDA WAKE ANGLE 2
 LAMBDA WAKE MAXIMUM DEFECT

FUSELAGE 1
 FUSELAGE 2
 FUSELAGE 3
 FUSELAGE 4

.....INTERFERENCE CONSTANTS ON HULL.....

A CONSTANT
B CONSTANT

-----GROUND ON HULL CONSTANTS

KGHA = .0100E+01
KGMH = .0100E+01

-----OPTION 1 ON HULL

KRHA1 = 0.
KRHA2 = .1000E+03 (SFC/FT)
KRHA3 = .1000E+02 (FT/AA2)
KRHA4 = .1000E+01
KRHA5 = .1500E+01

-----OPTION 2 ON HULL

KRA2 = 0.
KRA3 = .1000E+03 (SFC/FT)
KRA4 = .1000E+02 (FT/AA2)
KRA5 = .1000E+01
KRA6 = .1500E+01

-----OPTION 3 ON HULL

KRA7 = 0.
KRA8 = .1000E+03 (SFC/FT)
KRA9 = .1000E+02 (FT/AA2)
KRA10 = .1000E+01
KRA11 = .1500E+01

-----OPTION 4 ON HULL

KRA12 = 0.
KRA13 = .1000E+03 (SFC/FT)
KRA14 = .1000E+02 (FT/AA2)
KRA15 = .1000E+01
KRA16 = .1500E+01

-----OPTION 5 ON HULL

KRA17 = 0.
KRA18 = .1000E+03 (SFC/FT)
KRA19 = .1000E+02 (FT/AA2)
KRA20 = .1000E+01
KRA21 = .1500E+01

-----OPTION 6 ON HULL

KRA22 = 0.
KRA23 = .1000E+03 (SFC/FT)
KRA24 = .1000E+02 (FT/AA2)
KRA25 = .1000E+01
KRA26 = .1500E+01

-----OPTION 7 ON HULL

KRA27 = 0.
KRA28 = .1000E+03 (SFC/FT)
KRA29 = .1000E+02 (FT/AA2)
KRA30 = .1000E+01
KRA31 = .1500E+01

-----OPTION 8 ON HULL

KRA32 = 0.
KRA33 = .1000E+03 (SFC/FT)
KRA34 = .1000E+02 (FT/AA2)
KRA35 = .1000E+01
KRA36 = .1500E+01

ORIGINAL PAGE IS
OF POOR QUALITY

.....INTERFERENCE CONSTANTS ON TAIL.....

-----PROPRIETOR 1 ON TAIL CONSTANTS

KRTA1 = .5000E+02
KRTB1 = .2000E+02
KRTC1 = .1000E+02

-----PROPRIETOR 2 ON TAIL CONSTANTS

KRTA2 = .5000E+02
KRTB2 = .2000E+02
KRTC2 = .1000E+02

-----PROPRIETOR 3 ON TAIL CONSTANTS

KRTA3 = .5000E+02
KRTB3 = .2000E+02
KRTC3 = .1000E+02

-----PROPRIETOR 4 ON TAIL CONSTANTS

KRTA4 = .5000E+02
KRTB4 = .2000E+02
KRTC4 = .1000E+02

-----PROPRIETOR 1 ON TAIL CONSTANTS

KPTA1 = 0.
KPTB1 = 0.
KPTC1 = 0.

-----PROPRIETOR 2 ON TAIL CONSTANTS

KPTA2 = 0.
KPTB2 = 0.
KPTC2 = 0.

-----PROPRIETOR 3 ON TAIL CONSTANTS

KPTA3 = 0.
KPTB3 = 0.
KPTC3 = 0.

-----PROPRIETOR 4 ON TAIL CONSTANTS

KPTA4 = 0.
KPTB4 = 0.
KPTC4 = 0.

-----FUNCTION 01 TAIL CONSTANTS

KG1A = .5000E+02 (SFCa*2) / (U1a*2)
KG1B = .2000E+02 (SFCa*2) / (U1a*2)

ORIGINAL PAGE IS
OF POOR QUALITY

ORIGINAL PAGE 19
OF POOR QUALITY

.....ROTOR AND PROPELLER SPIN RATES.....

OMEGR1 =	25.2500 RAD./SEC.	ROTOR 1 SPIN RATE
OMEGR2 =	25.2500 RAD./SEC.	ROTOR 2 SPIN RATE
OMEGR3 =	25.2500 RAD./SEC.	ROTOR 3 SPIN RATE
OMEGR4 =	25.2500 RAD./SEC.	ROTOR 4 SPIN RATE
OMEGR1 =	120.2200 RAD./SEC.	PROPELLER 1 SPIN RATE
OMEGR2 =	120.2200 RAD./SEC.	PROPELLER 2 SPIN RATE
OMEGR3 =	120.2200 RAD./SEC.	PROPELLER 3 SPIN RATE
OMEGR4 =	120.2200 RAD./SEC.	PROPELLER 4 SPIN RATE

.....MECHANICAL FLIGHT CONTROL SYSTEM CONSTANTS.....

THETA1 =	10.0000 RADIANS	MAXIMUM ROTOR COLLECTIVE PITCH ANGLE
ALPHA1 =	10.0000 RADIANS	MAXIMUM ROTOR LATERAL CYCLIC PITCH ANGLE
BETA1 =	10.0000 RADIANS	MAXIMUM ROTOR LONGITUDINAL CYCLIC PITCH ANGLE
DELTA1 =	10.0000 RADIANS	MAXIMUM PROPELLER COLLECTIVE PITCH ANGLE
OLETA1 =	10000002 RADIANS	MAXIMUM TAIL AILERON DEFLECTION
OLETA2 =	10000002 RADIANS	MAXIMUM TAIL ELEVATOR DEFLECTION
OLETA3 =	10000002 RADIANS	MAXIMUM TAIL RUDDER DEFLECTION

Appendix B. FLIGHT CONTROL CHARACTERISTICS

Detailed information on the Helistat flight control system laws is very limited. Reference 7 presents an overview of the control system mixing laws along with a chart of maximum rotor and propeller forces resulting from full cockpit lever movements. Based on this information, a model of the Helistat control system was developed.

Figures a-c show a schematic drawing of the Helistat control system based on the discussion in Ref. 7. The significant features are:

- a. Forward velocity commands (δu) and yaw rate commands ($\delta \psi$) both induce forward commands to the helicopter propulsive command (BISC), resulting in rotor longitudinal cyclic (BIS_R) and propeller collective (θ_{OR}) deflections. The propeller collective (θ_{OP}) is a function of longitudinal command (BISC) and rotor collective (θ_{OR}) for each helicopter. In this way, the rotor/propeller mixing is a function of each isolated helicopter.
- b. Deflection of the master pilot's longitudinal control stick ($\delta \omega$) causes an increase in rotor collective on the rear two helicopters and a decrease in rotor collective on the front two helicopters for an aft stick movement. In addition the longitudinal stick causes a deflection of the elevator tail surface (δ_e).
- c. Deflection of the master pilot's lateral control stick ($\delta \phi$) causes an increase in rotor collective on the left two helicopters and a decrease in rotor collective on the right two helicopters. Also resulting from the lateral stick moment is a deflection of the rotor lateral cyclic (ALS_R) of all four helicopters as a function of individual rotor collective. This coupled control of rolling moments and side forces uses a "roll-to-translate" command logic. The information in Ref. 7 suggests that deflection of the lateral stick to its full travel produces full rolling moment authority in addition to lateral cyclic authority dependent on local rotor collective.

The roll-to-translate control logic may severely restrict the crosswind hover capability. As a result the Helistat's large metacentric height, very large roll control moments are necessary in order to maintain roll angles required in crosswind station-keeping. The lack of negative rotor collective travel severely restricts the obtainable rolling moment in lightly loaded configurations and thereby severely restricts the crosswind hover

capability of the vehicle. While it would be desirable to introduce some roll moment control through the lateral stick in order to reduce roll coupling associated with lateral translation command, the present use of full roll control authority does not appear to represent an optimum solution when only five cockpit controls are available.

An alternate solution would be to decouple the roll and side force controls by using a lateral translation button to control lateral cyclic in the same way that the forward translation button is used to control longitudinal cyclic. Then lateral stick movement could be retained to control full authority roll moment which would then be available to help augment the lateral hover capability once the full cyclic travel is used.

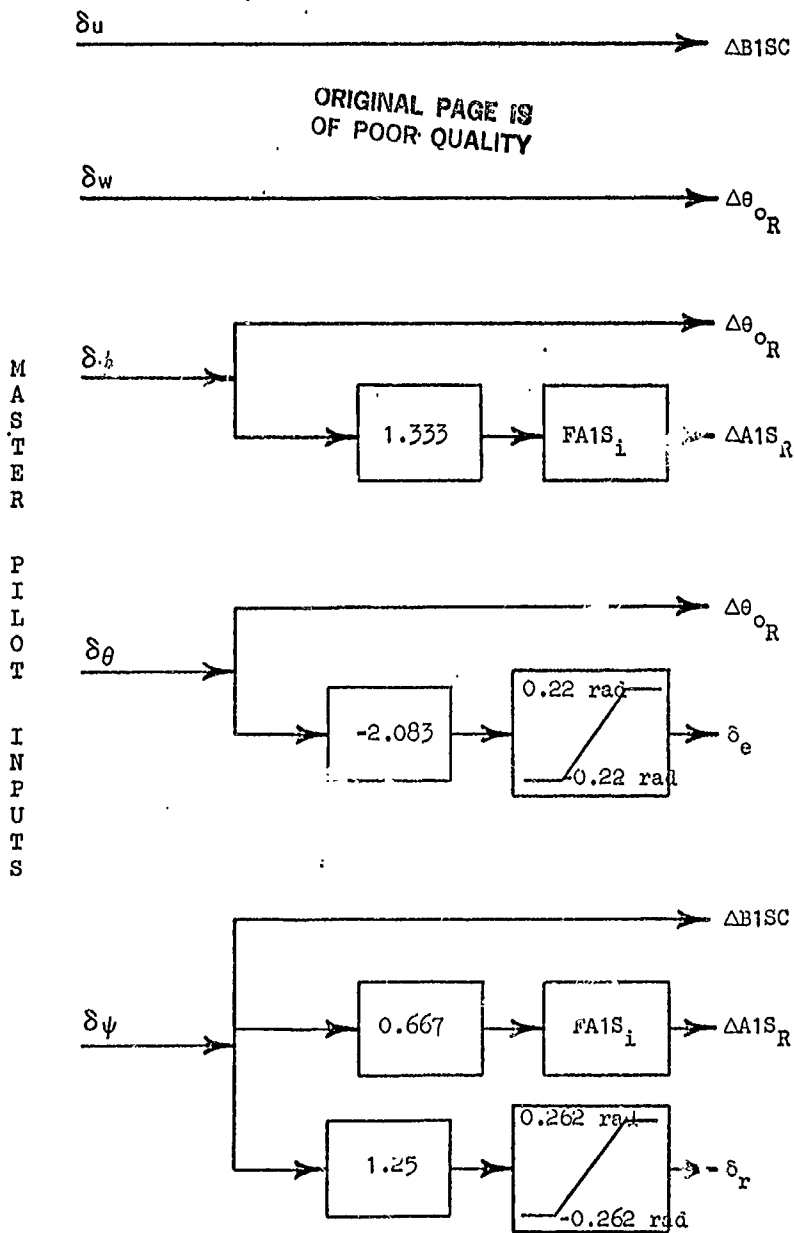
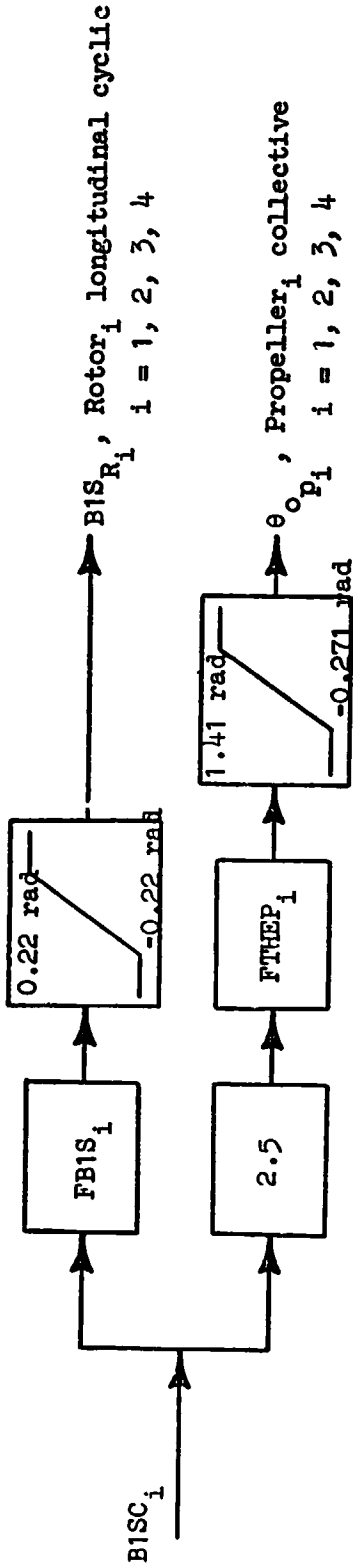


Figure a. Helistat Control System--Master I Control Logic

LPU-1, i = 1 (Front-Port)	LPU-2, i = 2 (Front-Starboard)
$BISC_i = \Delta BISC (\delta_u) + \Delta BISC (\delta_\psi)$	$BISC_i = \Delta BISC (\delta_u) - \Delta BISC (\delta_\psi)$
$AIS_{R_i} = \Delta AIS_R (\delta_\phi) + \Delta AIS_R (\delta_\psi)$	$AIS_{R_i} = \Delta AIS_{R_i} (\delta_\phi) + \Delta AIS_{R_i} (\delta_\psi)$
$\theta_{OR_i} = -\Delta\theta_{OR} (\delta_w) + \Delta\theta_{OR} (\delta_\phi) + \Delta\theta_{OR} (\delta_\psi)$	$\theta_{OR_i} = -\Delta\theta_{OR} (\delta_w) - \Delta\theta_{OR} (\delta_\phi) - \Delta\theta_{OR} (\delta_\psi)$
$BISC_i = \Delta BISC (\delta_u) + \Delta BISC (\delta_\psi)$	$BISC_i = \Delta BISC (\delta_u) - \Delta BISC (\delta_\psi)$
$AIS_{R_i} = \Delta AIS_R (\delta_\phi) - \Delta AIS_R (\delta_\psi)$	$AIS_{R_i} = \Delta AIS_{R_i} (\delta_\phi) - \Delta AIS_{R_i} (\delta_\psi)$
$\theta_{OR_i} = -\Delta\theta_{OR} (\delta_w) + \Delta\theta_{OR} (\delta_\phi) - \Delta\theta_{OR} (\delta_\psi)$	$\theta_{OR_i} = -\Delta\theta_{OR} (\delta_w) - \Delta\theta_{OR} (\delta_\phi) - \Delta\theta_{OR} (\delta_\psi)$
LPU-3, i = 3 (Aft-Port)	LPU-4, i = 4 (Aft-Starboard)

Figure b. Helistat Control System--LPU Control Mixing Logic



ORIGINAL PAGE IS
OF POOR QUALITY

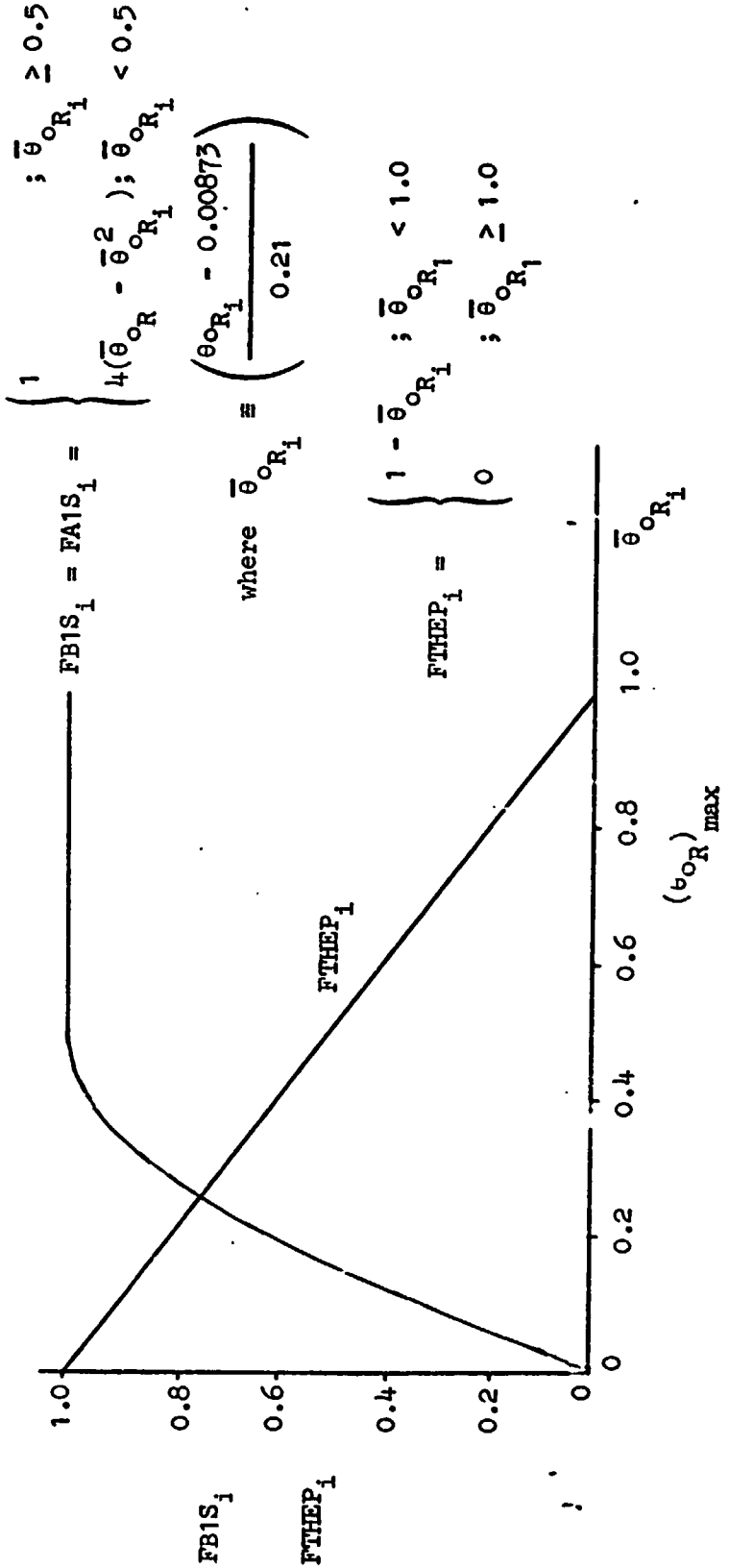


Figure c. Helistat Control System--Rotor Longitudinal Cyclic/Propeller Collective Mixing

- References:
1. Seckel, E., Stability and Control of Airplanes and Helicopters, Academic Press, New York, 1964.
 2. Hoerner, S. F., Fluid Dynamic Drag, published by author, 1965.
 3. Meyers, D. N., P. Kubicki, T. Parcuinski, A. Fairbanks, and F. N. Piasecki, Hybrid LTA Vehicle Controllability as Affected by Buoyancy Ratio, NASA CR-152,344, October 1979.
 4. Hoerner, S. F., Fluid Dynamic Lift, published by author, 1975.
 5. Schlichting, Hermann, and Erich Truckenbrodt (Translated by Henrich J. Ramm), Aerodynamics of the Airplane, McGraw-Hill International Book Company, New York, 1979.
 6. Tischler, Mark B., Robert F. Ringland, Henry R. Jex, Roger D. Emmen, and Irving L. Ashkenas, Flight Dynamics Analysis and Simulation of Heavy Lift Airships. Volume II: Technical Manual, Systems Technology, Inc., Technical Report No. 1151-2, Volume II, August 1982.
 7. Soergl, D. G., and K. R. Meenen, Piasecki Aircraft Company Progress Report PIAC 97-X-200-12 for the Period 1 January to 1 February, 1981,